

**UNCLASSIFIED**

---

---

**AD 289 298**

*Reproduced  
by the*

ARMED SERVICES TECHNICAL INFORMATION AGENCY  
ARLINGTON HALL STATION  
ARLINGTON 12, VIRGINIA



**20050204142**

---

---

**UNCLASSIFIED**

**Best Available Copy**

NOTICE: When government or other drawings, specifications or other data are used for any purpose other than in connection with a definitely related government procurement operation, the U. S. Government thereby incurs no responsibility, nor any obligation whatsoever; and the fact that the Government may have formulated, furnished, or in any way supplied the said drawings, specifications, or other data is not to be regarded by implication or otherwise as in any manner licensing the holder or any other person or corporation, or conveying any rights or permission to manufacture, use or sell any patented invention that may in any way be related thereto.

SP44-080200

63-1-4



**TECHNICAL INFORMATION SERIES**

289298

AD No. 289298  
FILE COPY

R62SD72

**THE ABLATION OF GRAPHITE  
IN DISSOCIATED AIR**

**I. THEORY**

**S.M. SCALA**

NOV 29 1962

289 298

**SPACE SCIENCES LABORATORY**

**GENERAL  ELECTRIC**

**SPACE DIVISION**



**SPACE SCI                      LABORATORY**

**AEROPHYSICS SECTION**

**THE ABLATION OF GRAPHITE IN DISSOCIATED AIR  
PART I: THEORY.\***

By

Sinclair M. Scala

\*Presented at the IAS National Summer Meeting,  
Los Angeles, California, June 19-22, 1962

R62SD72 - Class I  
September, 1962

MISSILE AND SPACE DIVISION

GENERAL  ELECTRIC

## TABLE OF CONTENTS

	PAGE
Abstract	1
I. Introduction	3
II. Symbols	8
III. The Reaction Rate Controlled Regime	14
IV. Diffusion Controlled Regime	24
V. Discussion of Results	32
VI. Conclusions	42
Acknowledgements	45
References	46
List of Tables	52
List of Figures	59

### ABSTRACT

An analysis is presented of the combustion of graphite in a high speed stream of dissociated air. Many features of the analysis are quite general and may be applied to the oxidation of different materials in arbitrary chemically reactive environments. However, because of the current interest in the hypersonic leading edge problem, numerical results are presented here which are directly applicable to surface oxidation at the leading edge region of fins and wings, and the nose cap of axially-symmetric hypersonic vehicles.

The reaction rate controlled regime and the transition-regime are first considered at length, and it is shown how the grade of graphite and its specific chemical properties influence the over-all oxidation rate.

It is then shown how the governing equations of change may be reduced to a coupled set of non-linear differential equations of the fifteenth order with variable coefficients and split boundary conditions. These differential equations are then utilized in treating the laminar, compressible, multicomponent, chemically reacting boundary layer in the diffusion controlled regime, and solutions are obtained for both the equilibrium and frozen gas flow chemical constraints. Numerical results are obtained on an IBM 704 digital computer, and correlated results are obtained for the heat transfer-

rate, the mass transfer rate and the skin friction coefficient for the complete range of suborbital hypersonic flight conditions of interest.

In addition, in order to establish a better understanding of the complex physicochemical processes which occur, many details of the structure of the boundary layer, including the variation of macroscopic gas velocity, gas temperature, chemical composition and chemical source terms through the boundary layer, are presented.

## I. INTRODUCTION

In considering the design of hypersonic lifting vehicles, special attention must be given to the leading edge surfaces which are exposed to sustained aerodynamic heating, and hence must function for long time periods at leading edge temperatures in the vicinity of  $4000^{\circ}\text{R}$  (Refs. 1-6).

A class of superior carbonaceous materials known as graphite immediately suggests itself because this form of carbon is a refractory material having high thermal shock resistance, good high temperature strength, excellent machinability, high thermal conductivity, a high sublimation temperature and a relatively low oxidation rate (see Table I).

The type of graphite which is in current use in industry is usually manufactured from carbon base materials, rather than mined as the natural substance, and hence is commonly called "artificial graphite". The latter is superior to either natural graphite or carbon, both of which have relatively low mechanical strength. It is noted that manufactured graphite is not one specific material, but a family of materials which are all essentially pure carbon. They differ from each in other in regard to the orientation of the crystallites, the grain size, the size and number of pore spaces, the degree of graphitization, and the level of impurities, which therefore lead to certain differences in the physical and chemical properties. Thus, the wide variation found in the properties of graphite can be attributed to the choice of starting materials, and to the degree of control during the manufacturing process. In reference 7 the reader will find a concise review of the properties and

applications of different grades of manufactured graphite.

Chemical reactions between carbon, coal, graphite and oxygen have been studied intensively for over one hundred years, and attention has been given to the reaction rate controlled, transition, and diffusion controlled oxidation regimes. Consequently, a voluminous literature exists, and excellent reviews on the mechanism of carbon oxidation have been written by Golovina (Ref. 8), Frank-Kamenetskii (Ref. 9), Arthur (Ref. 10), Townsend (Ref. 11), Strickland-Constable (Ref. 12), von Loon and Smeets (Ref. 13), Gerstein and Coffin (Ref. 14), Khitrin (Ref. 15), and Blakeley (Ref. 16). However, very little of this previous work applies to the environmental conditions encountered during hypersonic flight. Specific to the regime of greatest interest to the glide vehicle designer, little information is available other than the theoretical work of Scala (Refs. 17, 18), Lees (Ref. 19), Dennison and Dooley (Ref. 20), and Moore and Zlotnick (Ref. 21).

None of the previous work, either theoretical or experimental, considers the problem of determining systematically the relationship between mass loss, heat transfer, and viscous skin friction, as a function of the significant environmental parameters, such as the flight speed, the ambient pressure, the surface temperature and the model geometry.

In the study presented here, the hypersonic ablation of graphite is considered, and the heat transfer and mass transfer processes, and viscous

drag effects, which are experienced by hypersonic vehicles flying in the earth's atmosphere, are analyzed in detail. Although the analysis developed here is quite general, because of great current interest, numerical results have been obtained which are applicable to the leading edges of fins and wings, and at the forward stagnation point of axially-symmetric vehicles.

Upon introducing available experimental data on heterogeneous reaction kinetics (Refs. 22-26), the mass transfer and heat transfer rates will be determined at low surface temperatures, for the reaction rate controlled regime. At higher surface temperatures, the transition regime behavior will be determined utilizing the results obtained in the rate controlled and diffusion controlled regimes, by applying the concept of resistances to mass transfer in series. Since the heat transfer to the surface depends on the ratio of carbon monoxide to carbon dioxide at the surface, the recent data of Arthur (Ref. 27) and Bonnetain (Ref. 28) are also introduced.

At still higher surface temperatures, in the diffusion controlled regime, exact solutions will be obtained for the laminar flow of a compressible multicomponent chemically reacting gas over a reacting solid. It will be assumed that dissociated air produced by the upstream shock waves can be treated as a four component gas, consisting of oxygen and nitrogen atoms, and oxygen and nitrogen molecules. Since the primary combustion products include carbon monoxide and carbon dioxide, the total number of gaseous species considered is six. Therefore, the analysis requires the solution of a coupled set of non-linear partial differential equations, (including the conservation of mass, momentum, energy and chemical species) which is

of the fifteenth order, having split boundary conditions and variable transport and thermodynamic coefficients.

In the work presented here, as in earlier studies (Refs. 29,30), the transport properties of the individual atomic and molecular species will be calculated utilizing the rigid sphere and Lennard-Jones model, respectively. The thermodynamic properties of the pure species will be determined using the formulae of statistical mechanics. The transport and thermodynamic properties of the gaseous mixture will be evaluated during the solution of the problem, in terms of the gas composition, the pressure and the temperature.

Since the homogeneous rates of reaction of the various species present in the high temperature gas stream are not yet known precisely, calculations will be performed for the two limiting cases of "frozen" flow (infinitesimally slow gas phase reaction rates), and "local equilibrium" flow (infinitely fast gas phase reaction rates), which bracket the actual situation. It will be shown that, as in the case of hypersonic stagnation point heat transfer (Refs. 30 to 33), when the gas is in local equilibrium at the surface, for arbitrary hypersonic free stream conditions, both the overall rate of mass transfer and the net heat transfer rate are virtually independent of the rates of gas phase reaction in the diffusion controlled regime. This precludes the necessity of having an exact knowledge of gas phase kinetics.

In order to establish a better understanding of the physicochemical processes, many details of the structure of the multicomponent boundary

layer will be presented, including the variation of velocity, temperature, and gas composition as a function of distance from the surface. The zones in which chemical reactions occur in the gas phase and the magnitude of the various chemical source distributions  $w_1$  will be shown in detail. Calculations will also be made to determine the fraction of the heat transported to the reacting surface by the various fluid dynamic and molecular interaction processes. Finally, the magnitude of the viscous shear stress will be evaluated and correlated in the form of a skin friction coefficient.

Utilizing the graphical results, and the correlation formulas which will be presented here, one may predict the heat conducted into the solid, the mass loss from the leading edge and the skin friction coefficient, for a wide range of hypersonic flight conditions, i. e. Mach numbers in a range from 10 to 24, an altitude range from 10,000 ft. to 240,000 ft., and surface temperatures from the threshold range through  $6000^{\circ}\text{R}$ , for vehicles of arbitrary nose radius or wing leading edge radius, and angle of yaw.

## II. SYMBOLS

a, b	coefficients in equilibrium constant
Alt.	altitude
$C_f$	$\frac{\tau_w}{1/2 \rho_w u_e^2}$ , skin friction coefficient
$C_i$	mass fraction of species i
$C_{p_i}$	specific heat at constant pressure of species i
$\bar{C}_p$	$\sum_i C_i C_{p_i}$ , frozen specific heat of the mixture
$c_s$	specific heat of the solid
$\mathcal{D}_{ij}$	binary diffusion coefficient
$\mathcal{D}_{ii}$	self diffusion coefficient
$D_{ij}$	multicomponent diffusion coefficient
E	activation energy
f	similarity stream function
$f_\eta$	$u/u_e$ , dimensionless velocity
$h_i$	static enthalpy of species i, including chemical

$\Delta h_{f_i}^0$	standard heat of formation of species $i$ evaluated at $T_{ref}$ .
$h$	$\sum_i C_i h_i$ , static enthalpy of mixture
$\Delta H_{vap.}$	heat of vaporization
$\vec{j}_i$	$\vec{j}_i V_i$ , diffusion flux of species $i$
$J$	mechanical equivalent of heat
$k$	specific reaction rate
$k_0$	effective collision frequency
$K$	frozen thermal conductivity of the mixture
$K_{p_i}$	equilibrium constant of species $i$
$L_{i,j}$	$\frac{\rho \bar{c}_p D_{ij}}{K}$ , frozen Lewis number
$Li^T$	$\frac{\bar{c}_p D_i^T}{K}$ , frozen thermal Lewis number
$l$	$\rho \mu / \rho_w \mu_w$
$\dot{m}_w$	$\rho_w v_w = (\sum_i \rho_i v_i)_w$ , interphase mass transfer
$M_i$	molecular weight of species $i$

$\bar{M}$	$\sum_i X_i M_i$ , mean molecular weight of the mixture
N	number of chemical species
n	order of the reaction
$n_i$	number of moles of species i per unit volume
$P_i$	partial pressure of species i
P	$\sum_i P_i$ , static pressure
Pr	$\frac{\bar{c}_p \mu}{K}$ , frozen Prandtl number
$\Delta Q$	heat of reaction
$\tilde{Q}$	energy transfer function = $K \nabla T - \sum_i \rho_i V_i h_i$
Q	heat transfer rate
$Q^*$	effective heat of ablation
$\mathcal{R}$	universal gas constant
$R_B$	nose radius of body
$Re_x$	$\rho_w u_e x / \mu_w$ , Reynolds number based on x
(s)	solid state, condensed phase
t	time

$T$	temperature
$u$	x component of velocity
$v$	y component of velocity
$\underline{v}$	macroscopic stream velocity
$\underline{v}_i$	absolute velocity of species i
$\underline{v}_i$	diffusion velocity of species i
$v_\infty$	flight speed
$\dot{w}_i$	chemical source term, mass rate of production of species i by chemical reaction per unit volume per unit time
$X_i$	mole fraction of species i
$x, y, r$	body oriented coordinate system
$\dot{y}$	linear rate of surface recession
$\Lambda$	yaw angle
$\epsilon$	emissivity, depth of potential well
$\eta, \xi$	similarity variables
$\theta$	$T/T_e$ , dimensionless temperature

$\Theta$	characteristic vibrational temperature
$\mu_i$	viscosity coefficient of species $i$
$\mu$	viscosity of mixture
$\rho$	density
$\sigma$	Stefan - Boltzmann constant
$\tau$	viscous shear stress
$\sigma_{ij}$	collision diameter
$\psi$	stream function

Subscripts

AIR	treated as if the gas is dissociated air
c	condensed phase
cal.	calorimeter
e	outer edge of boundary layer
eq.	equilibrium
g	gaseous species
i	$i$ th species
rad.	radiation

s                    stagnation point

vap.                vaporization

w                    wall, interface

$\infty$                     upstream of shock, edge of boundary layer

$\eta$                     denotes differentiation with respect to  $\eta$

### III. THE REACTION RATE CONTROLLED REGIME

#### a) Mechanism of Surface Degradation

In an investigation of the behavior of graphite in dissociated air, one requires data on the nature and extent of the chemical reactions between carbon and the primary products of dissociated air, including atomic and molecular oxygen and nitrogen.

The recent work of Stieber (Ref. 34) indicates that nitrogen molecules can be considered chemically inert on carbon surfaces at temperatures as high as  $5400^{\circ}\text{R}$ . An early study by Strutt (Ref. 35) indicates that active nitrogen (primarily atomic nitrogen in the ground state) does not react with carbon at room temperature. In addition, Zinman (Ref. 36) who studied the interaction between atomic nitrogen and carbon at  $800^{\circ}\text{C}$ , did not detect measurable amounts of either cyanogen or paracyanogen. Consequently, one may conclude that at surface temperatures up to approximately  $2000^{\circ}\text{R}$ , no permanent carbon-nitrogen compounds are formed at a carbon surface. While experimental data is lacking at higher surface temperatures, it will be assumed that molecular nitrogen is chemically inert, and that atomic nitrogen undergoes heterogeneous recombination at a graphitic surface. Thus, if atomic nitrogen diffuses to the surface without undergoing gas phase recombination, then the graphite acts to catalyze the recombination of the atoms at the surface. In this study, therefore, surface degradation will be assumed to be primarily a consequence of a surface oxidation process. That is, chemical reactions between nitrogen and carbon, and mechanical effects such as spalling, will not be included in the theoretical calculation of the ablation rate, during hypersonic flight.

The carbon-oxygen reaction has been studied extensively for over one hundred years and hence, fortunately, although the mechanism is still not completely understood, sufficient experimental data exists upon which reasonable theoretical calculations may be based. The fact that graphite burns to form a mixture of carbon monoxide and carbon dioxide has been discussed in the literature, although there is some disagreement as to the sequence of the steps in the chemical reactions. At this time, as will be discussed, there is also some disagreement as to whether the overall reaction is first order with respect to the concentration of oxygen or of fractional order. It is interesting to note, however, that the widest differences in the oxidation behavior of the various grades of graphite are found at the lowest surface temperatures where the process is rate controlled, and these individual differences tend to disappear as the surface temperature rises.

Since the reaction between carbon and oxygen produces both CO and CO<sub>2</sub>, these products can be the result of either parallel or consecutive reactions. A number of different mechanisms are possible and these include the following:

1. The formation of both CO and CO<sub>2</sub> in a surface reaction between C(s) and O<sub>2</sub> or O.
2. The formation of CO<sub>2</sub> from C(s) and O<sub>2</sub> or O at the surface, followed by the dissociation of CO<sub>2</sub> to CO, O<sub>2</sub> and O in the gas phase, or reduction of CO<sub>2</sub> to CO at the surface.
3. The formation of CO at the surface from C(s) and O<sub>2</sub> or O, or C(s) and CO<sub>2</sub>, the CO being oxidized to CO<sub>2</sub> in the gas phase.

Measurements of the gas composition in the vicinity of an oxidizing carbon surface have been made by a number of different investigators, including Arthur (Ref. 27), Bonnetain (Ref. 28) and Snow et al (Ref. 37). They have verified that both species are detected adjacent to the surface, even at low surface temperatures, and that the ratio of the mass fraction of CO to CO<sub>2</sub> at the surface rises rapidly with increases in surface temperature. Their data can be represented by an Arrhenius equation,

$$\left( \frac{C_{CO}}{C_{CO_2}} \right)_w = k e^{-E/RT_w} \quad (1)$$

and are shown in Fig. 15.

It is noted that if the gas at the reacting surface had sufficient time to achieve thermochemical equilibrium during the low temperature oxidation process, then the composition of the gas could be determined from the equilibrium constant for the reaction,



Since the equilibrium constant for this reaction may be written in the form (see Table II),

$$K_{P_{CO}} = \frac{(P_{CO})^2}{P_{CO_2}} = e^{a - \frac{b}{T}} \quad (3)$$

it is not surprising that when the boundary layer solutions, which are based on the assumption of local thermochemical equilibrium at the surface, are compared with the experimental data of Arthur, Bonnetain, and Snow et al, see Fig. 15, the same general trend is exhibited. One may conclude

that either the gaseous CO-CO<sub>2</sub> system is actually never removed very far from an equilibrium state during oxidation, or that the experimental technique utilized by the investigators produces a shift toward the equilibrium composition.

Although these data cannot be utilized to rationalize the presence of any of the three suggested mechanisms, it is fortunate that the mass transfer and heat transfer at the surface can be predicted reasonably well without specifying the specific oxidation mechanism.

#### b) Reaction Rate Data

It is commonly accepted that the manner in which the oxidation of graphite proceeds depends on the type of graphite, the environmental conditions (e. g. the pressure, temperature, velocity and composition of the stream), the surface temperature, and at high surface temperatures, on the geometry of the model. The temperature at which a measurable mass loss first occurs, is called the threshold temperature (1000-1800° R) and is not a constant but depends on the partial pressure of the reacting gas at the surface.

At low surface temperatures, the mass loss increases rapidly with surface temperature, and the ablation rate is limited by the speed of the chemical processes, including adsorption, reaction and desorption.

At somewhat higher temperatures (1400-3200° R), the speed of the chemical processes is comparable to the rate at which fresh reactant is brought to the surface and the products of reaction are removed by convection and diffusion. Therefore, the overall process is in a transition regime, where the speed of the overall oxidation process is limited by the presence of two resistances in series, one chemical, and the second gas dynamic.

At temperatures above  $3200^{\circ}\text{R}$ , the chemical oxidation processes are overshadowed by the gas dynamic processes. In this diffusion controlled regime, the mass loss is relatively insensitive to the surface temperature. This result has been found experimentally for subsonic flow (Ref. 37) and will be demonstrated here for hypersonic flow.

Eventually, when the surface temperature is sufficiently high ( $5500\text{--}8000^{\circ}\text{R}$ ), the sublimation rate of carbon atoms and molecules can exceed the surface oxidation rate, and these species are then present in the gas phase.

Different investigators have studied one or more of these oxidation regimes. For example, the influence of environment upon the combustion rate of carbon has been studied by Hottel et al (Refs. 22, 39, 40), Chukhanov and Grozdovskii (Ref. 38), Gulbransen (Ref. 42), and more recently by Kuchta, Kant and Damon (Ref. 43).

The effect of the nature of the carbon on the oxidation rate has also been subject to investigation. For example, Riley (Ref. 44), and Smith and Polley (Ref. 45) have studied the effect of varying degrees of crystallinity of the carbon. Winslow et al (Refs. 46, 47) and Akamatsu et al (Ref. 48), investigated the relationship between the starting materials and the degree of graphitization. Wicke and Hedden (Refs. 49, 50), have postulated that for porous types of carbon, the diffusion of oxygen into the pores can be the rate controlling step in a transition regime between the rate controlled and diffusion controlled oxidation regimes; hence, the apparent activation energy is found to be half the true activation energy. However, Blakeley (Ref. 16), who investigated natural and artificial graphite under a variety of conditions, feels

that a pore diffusion mechanism is not required to explain his experimental data.

It has also been shown, e. g. Arthur (Refs. 51, 52), that impurities in the solid phase, such as sodium carbonate and zinc chloride, will augment the rate of oxidation in the reaction rate controlled regime. These experiments indicate that at relatively low temperatures, impurities tend to act as favorable sites, or catalytic agents, which promote the rate of reaction. Although little positive experimental data exists, one may anticipate that trace amounts of impurities in the gas phase will also influence the oxidation rate in the rate controlled regime.

With regard to the dependence of the rate of oxidation upon the pressure of oxygen in the stream, there is some experimental evidence that the reaction rate is first order with respect to oxygen pressure (Refs. 22, 49, 53). However, Frank-Kamenetskii (Ref. 9) has re-examined the experimental data of Parker and Hottel (Ref. 22) and has shown that the reaction rate can be interpreted to be of fractional order. Further, Semechkova and Frank-Kamenetskii (Ref. 54) have shown that the rate of reaction between carbon and carbon dioxide in the purely kinetic regime is lower than first order, while Klivanova and Frank-Kamenetskii (Ref. 55) have established that the reaction between carbon and oxygen is not first order, but fractional, lying between  $1/3$  and  $1/2$ .

Vulis (Ref. 26) tabulated a large amount of data on the kinetics of the reaction between carbon and oxygen or carbon dioxide. Upon applying an Arrhenius formula to the data, he found that the activation energy  $E$  varied between limits of 8 and 37 Kcal/mole for the carbon-oxygen reaction, and was approximately 2.2 times larger for the carbon-dioxide reaction. Vulis also

found that the logarithm of the specific reaction rate was a linear function of the activation energy, and hence, was led to the conclusion that the only experimentally determinable characteristic of a given variety of carbon is the activation energy of either of these reactions. However, Vulis' treatment of the data rests on the assumption that the true chemical kinetics at the surface follow a first order reaction, and it has been pointed out by Frank-Kamenetskii (Ref. 9) that this assumption lacks theoretical or experimental substantiation.

Examination of a large mass of experimental data (e. g. , Refs. 8, 9, 10, 11, 12, 13, 14, 15, 16, 21, 22, 23, 25, 26, 27, 38, 39, 40, 41, 42, etc...) indicates that in the reaction rate controlled regime, the oxidation process follows a rate law which may be written in the form:

$$\dot{m}_{w \text{ React.}} = k(P_{O_2})_w^n \quad (4)$$

where  $P_{O_2}$  is the partial pressure of the element oxygen near the surface,  $n$  is the order of the reaction, and  $k$  is the specific reaction rate.

As noted, there is some uncertainty about the precise value of  $n$ , as values in a range

$$0 \leq n \leq 1.0 \quad (5)$$

have been reported in the literature for different oxidation regimes. Also, as discussed, the specific reaction rate  $k$  is an exponentially increasing function of temperature whose precise magnitude is directly related to the type of graphite and its treatment during manufacture. Customarily, the

reaction rate constant is written in the standard Arrhenius form,

$$k = k_0 e^{-E/RT} \quad (6)$$

where the pre-exponential factor can vary over several orders of magnitude, and the activation energy has been reported to fall within the limits

$$8 \leq E \leq 60 \text{ Kcal./mole} \quad (7)$$

For example, Gulbransen and Andrew (Ref. 42), and Blyholder and Eyring (Ref. 43) report their data in the form of Eq. (6). Parker and Hottel (Ref. 22) utilized the form:

$$k = k_0 T^{-1/2} e^{-E/RT} \quad (8)$$

Vulis, (Ref. 26), obtained the empirical formula

$$k = k_0 T^{-1} e^{E(T-T^*)/RTT^*} \quad (9)$$

and Frank-Kamenetskii (Ref. 9) has suggested,

$$k = k_0 T^{-1/2} e^{E(T-T_0)/RT_0^2} \quad (10)$$

where the associated rate data for eqs. (6), (8), (9), and (10) appear in Table III. These data also appear in Fig. 16, where it is seen that the data of Parker and Hottel, and Vulis are based on a first order reaction, but the data of Gulbransen and Andrew, Frank-Kamenetskii, and Blyholder and Eyring, have been taken as following a one-half order reaction. This figure shows clearly that one can expect different grades of graphite to exhibit large differences in oxidation behavior in the rate controlled regime, i. e.,

$1400^{\circ}\text{R} \leq T_w \leq 3200^{\circ}\text{R}$ . However, fortunately at higher surface temperatures, the process becomes diffusion controlled and these large differences will no longer appear.

Although our subsequent results will usually be presented in a general form, wherever representative calculations are required to clarify the differences in behavior between grades of graphite having high and low specific reactivity, numerical calculations will be performed for "fast" and "slow" heterogeneous reactions, respectively. In particular, in the illustrative examples, we will utilize eqs. (4) and (6), with a value of  $n = 1/2$ . The values of the rate data will be arbitrarily taken as,

$$\text{"fast"} \left\{ \begin{array}{l} E = 44.0 \text{ kcal./mole} \\ k_o = 6.729 \times 10^8 \text{ lb./ft.}^{3/2} \text{ sec. atm.}^{1/2} \end{array} \right. \quad (11)$$

$$\text{"slow"} \left\{ \begin{array}{l} E = 42.3 \text{ kcal./mole} \\ k_o = 4.473 \times 10^4 \text{ lb./ft.}^{3/2} \text{ sec. atm.}^{1/2} \end{array} \right. \quad (12)$$

In the rate controlled regime, the rate of oxygen consumption adjacent to the surface is so low that the mass fraction of the element oxygen will be essentially the same as in the undisturbed stream. However, the atomic species will recombine in the low gas phase temperature regime adjacent to the surface and hence the mole fraction of molecular oxygen at the surface will be very nearly equal to its value in undissociated air. Further, the static pressure gradient in the reaction zone in a direction normal to the surface, is negligible. These considerations therefore enable us to write,

$$P_{O_2_w} = N_{O_2_w} P_w \quad (13)$$

for the reaction rate controlled regime only, and hence equation (4) becomes

$$\frac{(\dot{m}_w)_{\text{React.}}}{P_e^{1/2}} = k_o X_{O_2_w}^{1/2} e^{-E/RT_w} \quad (14)$$

where  $X_{O_2_w} = 0.21$  for undissociated air.

It is noted that if oxygen does reach the surface in the atomic state, reactions will occur, but at a somewhat different rate (Ref. 57), which will promote a shift in the transition regime.

#### IV. DIFFUSION CONTROLLED REGIME

##### a) Governing Equations

The non-linear partial differential equations of change for a multicomponent chemically reacting gas are derived, for example, in ref. 58, and include the conservation of mass, chemical species, momentum and energy as shown below:

$$\frac{\partial \rho}{\partial t} + \nabla \cdot (\rho \underline{v}) = 0 \quad (15)$$

where  $\underline{v}$  is the macroscopic stream velocity,

$$\frac{\partial \rho_i}{\partial t} + \nabla \cdot (\rho_i \underline{V}_i) = \dot{w}_i \quad (16)$$

where  $\dot{w}_i$  is the chemical source term,

$$\rho \frac{d\underline{v}}{dt} = \nabla \cdot \underline{\Pi} + \sum_i \rho_i \underline{F}_i \quad (17)$$

where  $\underline{\Pi}$  is the pressure tensor, and

$$\rho \frac{de}{dt} = -\nabla \cdot \underline{Q} + \underline{\Pi} : \underline{v\underline{v}} + \sum_i \rho_i \underline{V}_i \cdot \underline{F}_i \quad (18)$$

where  $e$  includes the chemical energy of formation.

Upon introducing the boundary layer approximation for the body-oriented coordinate system given in Figure 1, the conservation of mass becomes:

$$\frac{\partial}{\partial x} (\rho r u) + \frac{\partial}{\partial y} (\rho r v) = 0 \quad (19)$$

The conservation equation for species  $i$  becomes:

$$\rho M_i \left( u \frac{\partial B_i}{\partial x} + v \frac{\partial B_i}{\partial y} \right) + \frac{\partial}{\partial y} \left[ \sum_{j \neq i} \frac{M_i M_j}{\bar{M}^2} \rho D_{ij} \frac{\partial (\bar{M} B_j)}{\partial y} \right] = \dot{w}_i \quad (20)$$

The component of momentum becomes:

$$\rho u \frac{\partial u}{\partial x} + \rho v \frac{\partial u}{\partial y} = - \frac{\partial p}{\partial x} + \frac{\partial}{\partial y} \left( \mu \frac{\partial u}{\partial y} \right) \quad (21)$$

The  $y$  component of momentum is

$$\frac{\partial p}{\partial y} = 0 \quad (22)$$

The energy equation becomes:

$$\begin{aligned} \rho \bar{C}_p \left( u \frac{\partial T}{\partial x} + v \frac{\partial T}{\partial y} \right) &= u \frac{\partial p}{\partial x} + \mu \left( \frac{\partial u}{\partial y} \right)^2 \\ + \frac{\partial}{\partial y} \left( k \frac{\partial T}{\partial y} \right) - \sum_i c_{p_i} \frac{\partial T}{\partial y} \left[ \sum_{j \neq i} \frac{M_i M_j}{\bar{M}^2} \rho D_{ij} \frac{\partial (\bar{M} B_j)}{\partial y} \right] \\ - \sum_i \dot{w}_i h_i \end{aligned} \quad (23)$$

#### b) Transport and Thermodynamic Properties

The transport coefficients required for the definition of the physical problem include the coefficient of viscosity for each of the  $n$  pure species,  $(n^2 - n)/2$  symmetric binary diffusion coefficients, and  $n$  self diffusion coefficients. These properties may be calculated from the following equations (ref. 58).

$$\mu_i = \frac{5}{16} \frac{\sqrt{\pi m k T}}{\pi \sigma_i^2 \Omega^{(2,2)*}} \quad (24)$$

$$D_{ij} = \frac{3}{16} \frac{\sqrt{2\pi k^3 T^3 / \mu_{ij}}}{P \pi \sigma_{ij}^2 \Omega^{(1,1)*}} \quad (25)$$

which are the rigorous kinetic theory formulae for the viscosity and the diffusion coefficients respectively. In order to evaluate these properties one requires a knowledge of the collision diameter  $\sigma$ , and the collision integral  $\Omega^*$  as a function of  $T^*$ , the reduced temperature, where  $T^* = kT/\epsilon$ .

In the above, the symbol  $\mu_{ij}$  is the reduced mass given by:

$$\mu_{ij} = \frac{m_i m_j}{m_i + m_j} \quad (26)$$

and the collision diameter by:

$$\sigma_{ij} = \frac{1}{2} (\sigma_i + \sigma_j) \quad (27)$$

Note further that the constants to be utilized in the above equations are given in Table IV and the resulting transport properties of the pure species which are based on the Rigid Sphere and the Lennard Jones 6:12 potential respectively are shown in Figures 2, 3 and 4.

c) Similarity Transformation

Upon introducing the Mangler-Dorodnitsyn transformations

$$\eta = \frac{u_e \rho_e}{\sqrt{2 \xi}} \int_0^y r \frac{\rho}{\rho_e} dy \quad (28)$$

$$\xi = \int_0^x \rho_w \mu_w u_e r^2 dx \quad (29)$$

and assuming that local similarity holds, then equations (19) through (23) may be reduced to a set of ordinary non-linear equations. The diffusion equation becomes:

$$\left[ \frac{l}{Pr} \sum_{j \neq i} \frac{M_i M_j}{\bar{M}^2} L_{ij} (\bar{M} B_j)_\eta \right]_\eta - f M_i B_{i\eta} - \frac{2 \xi}{u_e \xi_x} \frac{\bar{w}_i}{\rho} = 0 \quad (30)$$

The conservation of momentum becomes:

$$(l f_{\eta\eta})_\eta + f f_{\eta\eta} + \beta \left[ \frac{\rho_e}{\rho} - f_\eta^2 \right] = 0 \quad (31)$$

while the energy equation becomes:

$$\begin{aligned} & \left( \frac{\bar{c}_p l}{Pr} \theta_\eta \right)_\eta + \bar{c}_p f \theta_\eta - \sum_i c_{p_i} \theta_\eta \left[ \frac{l}{Pr} \sum_{j \neq i} \frac{M_i M_j}{\bar{M}^2} L_{ij} X_{j\eta} \right] \\ & + \frac{u_e^2}{T_e} \left[ l (f_{\eta\eta})^2 + \beta f_\eta \left( \theta - \frac{\rho_e}{\rho} \right) \right] - \frac{2 \xi}{\xi_x u_e} \frac{\sum_i \bar{w}_i h_i}{\rho T_e} = 0 \end{aligned}$$

(32)

F E T Y A F L M L F +  
d) Chemical Constraints and Boundary Conditions

It will be assumed here that the total number of dominant species present in the gas phase is six, including atomic and molecular oxygen, atomic and molecular nitrogen and the combustion products, carbon monoxide and carbon dioxide. Thus, there are six unknown chemical source terms  $\dot{W}_i$  and six unknown concentrations  $X_i$  at each point within the boundary layer.

At the surface, there are six unknown concentrations which must satisfy the chemical constraints imposed by the surface oxidation process.

Let us therefore consider the chemical constraints. The conservation of chemical species in the gas phase requires that

$$\sum_i \dot{W}_i = 0 \quad (33)$$

Since it has been assumed that the nitrogen species do not react with oxygen or carbon to form permanent compounds (i.e. the formation of NO or CN is not considered explicitly), one may also write for the case of thermochemical equilibrium

$$\dot{W}_N + \dot{W}_{N_2} = 0 \quad (34)$$

while combustion stoichiometry requires

$$\dot{w}_O + \dot{w}_{O_2} = -\frac{4}{11} \dot{w}_{CO_2} \quad (35)$$

$$\dot{w}_{CO} = -\frac{7}{11} \dot{w}_{CO_2} \quad (36)$$

For the case of frozen reactions one has

$$\dot{w}_i \equiv 0 \quad (37)$$

The surface boundary conditions on velocity and temperature may then be written:

$$f_{\eta_w} = \frac{u_w}{u_e} = 0 \quad (38)$$

$$f_w = -\dot{m}_w \frac{r\sqrt{2\xi}}{\xi_x} \quad (39)$$

$$\theta_w = \frac{T_w}{T_e} \quad (40)$$

The boundary conditions on the composition are obtained from the simultaneous solution of the equilibrium constants:

$$K_{P_{O_w}} = \frac{X_{O_w}^2 P}{X_{O_2 w}} \quad (41)$$

$$K_{P_{N_w}} = \frac{X_{N_w}^2 P}{X_{N_2 w}} \quad (42)$$

$$K_{P_{CO_w}} = \frac{X_{CO_2 w} P}{X_{O_w} X_{CO_w}} \quad (43)$$

It is also noted that in the theoretical models considered here, the nitrogen atoms are permitted to recombine on the surface, one may also write:

$$(\dot{m}_N + \dot{m}_{N_2})_w = 0 \quad (44)$$

and hence since

$$\dot{m}_w = \left( \sum_i \dot{m}_i \right)_w \quad (45)$$

one immediately obtains for the oxidation rate

$$\dot{m}_w = \frac{(j_O + j_{O_2} + j_{CO} + j_{CO_2})_w}{1 - (C_O + C_{O_2} + C_{CO} + C_{CO_2})_w} \quad (46)$$

The boundary conditions at the outer edge of the boundary layer

for velocity and temperature are given by:

$$\lim_{\eta \rightarrow \infty} f_\eta = \lim_{\eta \rightarrow \infty} \theta = 1.0 \quad (47)$$

and in addition, one has  $n-1$  relations of the form:

$$\lim_{\eta \rightarrow \infty} X_i = X_i^e \quad (48)$$

The total number of boundary conditions therefore equals the order of the mathematical system.

## V. DISCUSSION OF RESULTS

In this section, the results of the theoretical investigation will be discussed in detail. As already noted, a convenient coordinate system for the study of the hypersonic laminar boundary layer is the body-oriented coordinate system shown in Figure 1. In order to treat the problem in the absence of experimental data, the high temperature transport coefficients and thermodynamic properties of the reacting species were determined theoretically utilizing kinetic theory, statistical thermodynamics and the gas constants given in Table IV. The theoretical results are shown in Figures 2 to 6. Here it is remarked that the properties of the gas mixture have been treated as variable and were computed through the boundary layer as a function of both the local gas composition and the properties of the pure species at the local gas temperature. Thus, since the gas properties are computed as part of the solution, one does not require simplifying assumptions such as constant Prandtl and Lewis numbers, or a constant product of density and viscosity in order to solve the problem. That is, once an appropriate intermolecular force law between a pair of molecules has been selected, one may immediately calculate uniquely the properties of the pure species, and then one may proceed to utilize these to determine the mixture properties as dictated by the chemistry of the particular physical problem.

In Figure 7 are shown typical values of the variation of the normalized product of density and viscosity through the boundary layer, as a function of

the stretched normal coordinate. Qualitatively, the trends are the same, namely that the quantity  $\rho/\rho_w$  decreases with increasing gas temperature. This may readily be explained as follows. In a dissociating gas boundary layer, which is locally a constant pressure layer, the density ratio is given by:

$$\frac{\rho}{\rho_w} = \frac{\bar{M}}{\bar{M}_w} \frac{T_w}{T} \quad (49)$$

and hence, clearly, the decrease in molecular weight with increasing temperature produces a smaller density ratio  $\rho/\rho_w$  (greater density change) with increasing gas temperature than will occur in a non-dissociating gas. This is particularly true for the case of the mass transfer of foreign species at the surface having a higher molecular weight than the primary gas species. Since the increase in viscosity with gas temperature is less than linear, the increase in the viscosity ratio  $\mu/\mu_w$  with increasing temperature does not compensate for the decrease in the density ratio  $\rho/\rho_w$ . Thus, the larger the ratio of the gas temperature at the edge of the boundary layer to that at the wall, the smaller will be the value of the normalized  $\rho\mu$  product at the outer edge of the boundary layer, and the poorer the assumption that  $\rho\mu$  is constant. This is shown in curves 1, 2, and 5 of Figure 7, which were calculated for the chemical constraint of local equilibrium flow. By way of further comparison, curve 3 of Figure 7 was computed for the case of equilibrium dissociated air (no graphite combustion), and curve 4 was calculated for the chemical constraint of frozen

reactions, all for the same flight conditions. It is seen that under certain conditions the density-viscosity variation may have nearly the same behavior for both the frozen flow and local equilibrium constraints, (compare curves 4 and 5), although the other gas properties such as, for example, the thermal conductivity, do not.

When one defines the Prandtl number of the gas in terms of the frozen specific heat of the mixture  $\bar{c}_p$ , the viscosity of the mixture  $\mu$  and the frozen thermal conductivity  $K$ , one obtains the results shown in Figure 8. Here, the value of the Prandtl number of the gas at the surface versus the surface temperature over a wide range of pressures. It appears from this figure that the presence of carbon dioxide at the surface at the lower surface temperatures acts to increase the Prandtl number. At a given value of the temperature, the effect of a pressure increase is to decrease the dissociation of carbon dioxide and hence the shifting equilibrium composition with increasing pressure results in an increase in the Prandtl number. The total effect, however, is less than four percent since the maximum mole fraction of carbon dioxide is less than 0.2. Of greater interest are the Lewis numbers which have been defined here in terms of the multicomponent diffusion coefficients  $D_{ij}$ , which, unlike the binary diffusion coefficients  $D_{ij}$ , are not symmetric. Consequently, since all other gas properties which appear in the multicomponent Lewis number are not dependent on the particular pair of particles involved in a given binary encounter, while the multicomponent diffusion coefficients

are both temperature and composition dependent. It is clear that there are generally  $n^2$  values of the Lewis number; in this case there are 30, of which 12 representative values are shown in Figure 9.

When the boundary layer equations are integrated subject to the appropriate boundary conditions, one obtains the velocity distribution, the temperature distribution and the distribution of species through the layer.

These are shown in Figure 10 and 11. Corresponding chemical source terms are shown in Figure 12.

Since preferential diffusion can occur, it is found that the ratio of the element oxygen to the element nitrogen at the surface is not necessarily equal to its value at the edge of the boundary layer, and is in fact an eigenvalue of the mathematical system. This is shown in Figure 13 and 14.

In the rate controlled regime, it is found that the ratio of the mass fraction of carbon monoxide to the mass fraction of carbon dioxide is a sensitive function of surface temperature, which increases with increasing surface temperature. This can be shown to be the case from both theoretical and experimental considerations and is demonstrated in Figure 15.

Examination of the literature indicates that the reaction rate controlled mass transfer is also a very sensitive function of surface temperature and in fact as many different activation energies and specific reactivities have been reported in the literature as there are combinations of investigators and grades of graphite.

The work of five different investigators is shown in Figure 16. The exponential dependence of the oxidation rate on surface temperature is clearly seen which leads to the usual Arrhenius representation.

Typical values of the reaction rate results therefore appear in Figure 17 for a representative flight condition.

In Figure 18 we have shown the correlated results for the mass transfer of oxidation products for both the rate controlled and diffusion controlled regimes. When the surface temperature exceeds 3000°R the oxidation rate levels off and becomes insensitive to the magnitude of surface temperature, simply because the mass loss is controlled by the diffusion of oxygen-bearing species to the surface rather than the specific reactivity of graphite.

Upon making use of the concept of the sum of resistances in series, one may write:

$$\dot{m}_w = \frac{1}{\frac{1}{\dot{m}_w \text{Diff.}} + \frac{1}{\dot{m}_w \text{React.}}} \quad (50)$$

where the reaction term predominates at low surface temperatures and diffusion predominates at high surface temperatures. This equation was utilized in calculating the transition regime in Figure 19.

In order to obtain an over-all feeling for the combined effect of pressure and surface temperature on the oxidation rate, Figure 20 has been prepared. Here it is seen that there are 4 different regimes for the oxidation of graphite. In

this paper we have considered the first three regimes from the reaction rate controlled regime through the transition to diffusion controlled oxidation.

It is also of interest to consider the heat transfer into the solid graphite. It is instructive to compare the heat transfer to the solid graphite to the heat transfer to an inert surface.

This is shown in Figure 21, where it is seen that one may not insist that the process remains diffusion controlled down to the lowest surface temperature, which would result in an overestimate of the heat transfer. It is clear that as surface temperature decreases, the heat transfer must reduce to the aerodynamic heating, since the oxidation rate decreases exponentially with decreasing surface temperature.

Since the total "convective" energy transfer including conduction, convection diffusion and chemical reaction is given by:

$$-Q_w = \left[ K \frac{\partial T}{\partial y} - \sum_i \rho_i v_i h_i \right]_w \quad (51)$$

it is instructive to examine Figure 22 which compares the results for both the equilibrium and frozen gas chemical constraints. It is seen that although the separate contributions differ from each other, the total heat transfer is independent of chemical constraints provided only that the surface is purely catalytic.

In Figure 23, we have shown the correlated heat transfer for the heat conducted into solid graphite for an axially symmetric object, however, numerical results have also been obtained for a two-dimensional body and the heat transfer

rate was correlated by means of the following equation:

$$\frac{Q_w \sqrt{2R_B}}{P_e^{1/2} f(\Lambda)} \left[ \frac{f(\Lambda)}{\sqrt{2}} \right]^\delta = 33.3 + 0.0333(H_e - h_{wAir}), \frac{\text{BTU}}{\text{ft.}^{3/2} \text{sec. atm.}^{1/2}} \quad (52)$$

where  $f(\Lambda)$  represents the effects of yaw,  $\delta$  is the kronecker  $\delta$  such that this equation applies to both axially symmetric ( $\delta = 1$ ), and two-dimensional ( $\delta = 0$ ) geometries.  $P_e$  is the local static pressure at the outer edge of the boundary layer,  $H_e$  is the stagnation enthalpy and  $h_{wAir}$  is the static enthalpy of the gas evaluated at the surface temperature and treated as if it were air, expressed in BTU/lb. Figures 23 and 24 represent different ways of depicting the correlated heat transfer.

If one utilizes the horizontal portion of the graph shown in Figure 25 for  $\dot{m}_w$ , one obtains the following result for the diffusion controlled mass loss:

$$\frac{(\dot{m}_w \text{ Diff.}) \sqrt{2R_B}}{P_e^{1/2} f(\Lambda)} \left[ \frac{f(\Lambda)}{\sqrt{2}} \right]^\delta = 6.2 \times 10^{-3} \frac{\text{lb.}}{\text{ft.}^{3/2} \text{sec. atm.}^{1/2}} \quad (53)$$

Note that equation (14), which represents the reaction rate controlled mass loss is independent of the geometric factors whereas the diffusion controlled mass loss, equation (53), is not.

It is noted that in both equations (52) and (53), the effects of yaw, which act to decrease the heat and mass transfer, appear in the function  $f(\Lambda)$ . Although more complicated correlations have been suggested, (Ref. 59), the author believes that the following approximation is satisfactory.

It is of some interest to calculate the so-called "effective heat of ablation". This may be done readily for the diffusion controlled regime by taking the ratio of  $Q_w$  to  $\dot{m}_w$ , and one obtains a result which is independent of the geometry of the body, that is:

$$Q^* = 5370 + 5.37 (H_w - h_{w,air}), \text{ BTU/lb.} \quad (54)$$

It should be noted that since the driving force for the mass transfer process is not really the heat transfer but rather the oxidation process, one should not be surprised that the effective heat of ablation is of the order of 70,000 BTU/lb. at orbital velocity. It must be understood that graphite is actually an excellent sink material which also undergoes surface oxidation.

In this paper we have also determined the surface shear stress  $\tau_w$ , defined by

$$\tau_w = \mu_w \left( \frac{\partial u}{\partial y} \right)_w \quad (55)$$

and a typical result is shown in Figure 26.

Upon defining a local skin friction coefficient  $c_{f_w}$ :

$$c_{f_w} = \frac{\tau_w}{\frac{1}{2} \rho_w u_e^2} \quad (56)$$

and a Reynolds number based on  $x$ :

$$Re_w = \frac{\rho_w u_e x}{\mu_w} \quad (57)$$

one also obtains the correlated results shown in Figure 27. For purposes of comparison, results are also given for the skin friction coefficient in the absence of surface oxidation.

Finally, it may be of some interest to be able to rapidly estimate the surface temperature as a function of environmental conditions such as  $H_e$  and  $P_e$ . In general, one has:

$$Q_w + \sigma(\epsilon_g T_g^4 - \epsilon_w T_w^4) = (K \frac{\partial T}{\partial y})_{\text{Solid}} \quad (58)$$

where  $Q_w$  is the total convective heat flux to the surface,  $\sigma \epsilon_g T_g^4$  represents radiation to the surface from the hot gas cap,  $\sigma \epsilon_w T_w^4$  is the reradiation from the surface and  $(K \frac{\partial T}{\partial y})_{\text{solid}}$  is the heat conducted into the interior of the solid graphite.

If one assumes that radiation equilibrium obtains, the right hand side of equation (58) may be set equal to zero. In this case, one may write that the radiation equilibrium temperature is:

$$T_w^{\text{Rad. Eq.}} = \left[ \frac{Q_w + \sigma \epsilon_g T_g^4}{\sigma \epsilon_w} \right]^{1/4} \quad (59)$$

In general, for suborbital flight,  $\sigma \epsilon_g T_g^4 \ll Q_w$  and if this term is neglected one obtains the typical results shown in Figure 28 for a value of the radiation parameter  $\epsilon_w \sqrt{R_B} = 0.85 \text{ ft.}^{1/2}$ .

## VI. CONCLUSIONS

A study of the ablation of graphite indicates that one may recognize at least four distinct acrothermochemical regimes. As the surface temperature rises into the threshold range, the mass transfer process is initially rate controlled and follows a fractional (half order) reaction law. At surface temperatures of approximately  $1400^{\circ}\text{R} < T_w < 3200^{\circ}\text{R}$ , a transition regime exists and the overall rate of the process is controlled both by chemical and gas dynamic factors. At higher surface temperatures extending through  $6000^{\circ}\text{R}$ , the process is diffusion controlled and the rate of mass loss from the surface is limited by the rate at which oxidizing species diffuse to the surface. Finally, there is a regime in which the surface temperature is sufficiently high so that the sublimation rate exceeds the surface oxidation rate, and carbon atoms and molecules are present in the gas phase.

In the rate controlled and transition regimes, the ablation rate of graphite is a sensitive function of the surface temperature, and depends critically on the specific reaction rate which has an exponential temperature dependence. It is in the low surface temperature regime that one can distinguish between different grades of graphite, since the activation energy and the effective collision frequency depend on the molecular structure of the particular carbonaceous material. Therefore, unless one has an independent knowledge of the chemical kinetics of the combustion process for the specific carbonaceous material, one cannot make a precise

prediction of the oxidation rate for surface temperatures below  $3200^{\circ}\text{R}$ .

The thermochemical response of graphite in the transition regime can be easily synthesized from a knowledge of its behavior in the purely rate controlled and diffusion controlled regimes. A more precise study of the transition regime itself does not appear to be warranted at this time because of an incomplete knowledge of certain of the chemical factors, e. g. the  $\text{CO}/\text{CO}_2$  ratio.

In the diffusion controlled regime, it is found that the ablation rate is proportional to the square root of the pressure and is essentially independent of surface temperature. It is further noted that for surface temperatures above  $3200^{\circ}\text{R}$ , barring spalling effects, the mass loss is theoretically independent of the grade of the graphite. The main uncertainty resides in the somewhat arbitrary selection of the high temperature transport properties due to the lack of experimental data for any of the six gaseous species present at the temperatures of interest. However, judging by a comparison between theory and experiment for stagnation point heat transfer in the absence of mass transfer, it is estimated that the uncertainty in the transport properties introduces no more than approximately a fifteen percent error in the present final results.

A study of the calculated results indicates that in the diffusion controlled regime, the heat and mass transfer are independent of the rates of the homogeneous reactions, provided that the heterogeneous reactions are rapid. That is, when it was assumed that thermochemical equilibrium was

obtained at the surface, but not necessarily throughout the boundary layer, both the "frozen reactions" and "local equilibrium" chemical constraints yielded essentially identical results.

In considering the heat conducted into the solid, one notes that the separate contributions of convection, diffusion, conduction and radiation must be included. In this study, it was found that the net heat transfer, including combustion effects, exceeds the aerodynamic heat transfer. One may conclude therefore, that the exothermicity of the oxidation reactions exceeds the decrease in heat transfer due to mass transfer cooling effects, (thickening of the boundary layer), which results in a net increase in the heat transfer to the solid. However, this increase is usually less than ten percent for the full range of interest.

With regard to viscous drag effects, it is concluded that for the hypersonic flight regime the reduction in skin friction due to the mass transfer of oxidation products does not appear to be significant, and is of the order of seven percent or less.

## ACKNOWLEDGEMENTS

The author wishes to acknowledge the fruitful discussions held with his colleagues, Dr. Guido Vidale, Dr. Albert Myerson and Dr. Joseph Farber, and the assistance of Charles Baulknight in the calculation of the transport properties. In addition, the author wishes to thank Leon Gilbert for his valued assistance in the analysis, in the preparation of the graphs and in the computations, and Messrs. Frank Bosworth and Paul Gordon, who programmed the differential equations for the IBM 704 digital computer.

This paper is based on work performed under the auspices of the United States Air Force, Ballistic Missiles Division, Contract No. AF04(647)-269.

#### REFERENCES

1. S. M. Scala and E. J. Nolan, Aerothermodynamic Feasibility of Graphite for Hypersonic Glide Vehicles, Re-entry and Vehicle Design, Vol. 4, Proc. of the Fifth Symposium on Ballistic Missile and Space Technology, Academic Press, New York, 1960, pp. 31-63.
2. E. J. Nolan and S. M. Scala, Aerothermodynamic Behavior of Pyrolytic Graphite During Sustained Hypersonic Flight, ARS Journal Vol. 32, No. 1, January 1962, pp. 26-35.
3. A. J. Hanawalt, A. H. Blessing, and C. M. Schmidt, Thermal Analysis of Stagnation Regions with Emphasis on Heat Sustaining Nose Shapes at Hypersonic Speeds, J. Aero/Space Sci., Vol. 26, No. 5, May 1959, p. 257.
4. F. M. Anthony and H. A. Pearl, Selection of Materials for Hypersonic Leading Edge Applications, IAS Preprint 59-111, June 1959.
5. A. Flathers, Some Aerothermodynamic Considerations of Hypervelocity Vehicles, ARS Preprint 858-59, Presented at the ARS Semi-Annual Meeting, San Diego, Calif., June 8-12, 1959.
6. R. T. Swann, An Engineering Analysis of the Weights of Ablating Systems for Manned Re-entry Vehicles, Re-entry and Vehicle Design, Vol. 4, Proc. of the Fifth Symposium on Ballistic Missile and Space Technology, Academic Press, New York, 1960, pp. 65-86.
7. Anon. The Industrial Graphite Engineering Handbook, National Carbon Co., 1959.
8. Golovina, E. S. and Khaustovich, G. P. The Interaction of Carbon with Carbon Dioxide and Oxygen at Temperatures up to 3000°K, Eighth Symposium on Combustion, Williams and Wilkins Co., 1962, pp. 784-792.
9. Frank-Kamenetskii, D. A., Diffusion and Heat Exchange in Chemical Kinetics, Princeton University Press, 1955.

10. Arthur, J.R. BCURA, Vol. 8, 1944, p. 202.
11. Townsend, J. Chem Phys., Vol. 47, 1950, p. 315.
12. Strickland-Constable, R.F., J. Chem Phys., Vol. 47, 1950, p. 322.
13. von Loon, W. and Smeets, H.H., Fuel, Vol. 29, 1950, p. 119.
14. Gerstein, M. and Coffin, K.P., Combustion of Solid Fuels Section K, Combustion Processes, Vol. II, High Speed Aerodynamics and Jet Propulsion, Princeton University Press, 1956.
15. Khitrin, L.N., Fundamental Principles of Carbon Combustion and Factors Intensifying the Burning of Solid Fuels, Sixth Symposium on Combustion, Reinhold Publ. Corp., New York, (1956), pp. 565-573.
16. Blakeley, T.H. The Gasification of Carbon in Carbon Dioxide and Other Gases at Temperatures Above 900°C, Proceedings of the Fourth Conference on Carbon.
17. Scala, S.M., Surface Combustion in Dissociated Air, Jet Propulsion, Vol. 29, 1958, pp. 340-341.
18. Scala, S.M., A Study of Hypersonic Ablation, Proceedings of the Tenth I.A.F. Congress, London, 1959, Springer Verlag.
19. Lees, L., Convective Heat Transfer with Mass Addition and Chemical Reactions, Third AGARD Colloquium on Combustion and Propulsion, Palermo, Sicily Pergamon Press, 1959.
20. Denison, M.R. and Dooley, D.A., Combustion in the Laminar Boundary Layer of Chemically Active Sublimators, Aeronutronic Systems Report U-119, Sept., 1957.
21. Moore, J.A. and Zlotnick, M., Combustion of Carbon in an Air Stream, AVCO, RAD -TR-9-60-32, Dec. 1960.
22. Parker, A.S. and Hottel, H.C., Combustion Rate of Carbon Ind. Eng. Chem., Vol. 28, No. 11, Nov. 1936. pp. 1334-1341.

23. Culbransen, E. A. and Andrew, K. F., "Reactions of Artificial Graphite", Ind. Eng. Chem., Vol. 44, No. 5, 1952, pp. 1034-1041.
24. Blyholder, G. and Eyring, H. J. Chem Phys. Vol. 61, 1957, p. 61.
25. Blyholder, E. A., "Mechanism of the Oxidation of Graphite at Temperatures of 425°C to 575°C", Ind. Eng. Chem., Vol. 44 No. 5, 1952, pp. 1045 -1051.
26. Vulis, L. A. "K raschetu absolyutnoi skorosti reakcii goreniya uglya", Zhur. Tekh. Fiz., Vol. 16, No. 1, 1946, pp. 83-88.
27. Arthur, J. R. and Wadsworth, K. D. BCURA, Vol. 8, 1944, p. 296.
28. Bonnetain, L., "Combustion de Graphites Artificiels Sous Basses Pressions D'Oxygene", Jour. Chim. Phys., 1959, Part I, pp. 266-276, Part II, pp. 486-494.
29. Scala, S. M. and Baulknight, C. W. "Transport and Thermodynamic Properties in the Hypersonic Laminar Boundary Layer, Part II" ARS Journal, Vol. 30, No. 4, May 1960, pp. 329-336.
30. Scala, S. M., "Hypersonic Heat Stagnation Point Heat Transfer to Surfaces Having Finite Catalytic Efficiency", Third U. S. Cong. Appl. Mech. 1958, pp. 799-806.
31. Lees, L., "Laminar Heat Transfer Over Blunt Bodies at Hypersonic Flight Speeds", Jet Propulsion, Vol. 26, 1956, pp. 259-269.
32. Fay, J. A., and Riddell, F. R., "Theory of Stagnation Point Heat Transfer in Dissociated Air", J. Aero. Sci., Vol. 25, 1958, pp. 78-85.

33. Scala, S.M., "The Injection Air into the Dissociated Hypersonic Laminar Boundary Layer", J. Aero. Sci., Vol. 25, No. 7, 1958, pp. 461-462.
34. Stieber, H.C. Private communication to W. Zinman.
35. Strutt, R.J., "A Chemically Active Modification of Nitrogen Produced by the Electric Discharge", Proc. Roy. Soc., A85, 1911, pp. 219-229.
36. Zinman, W.G., "Study of the Interaction Between Carbon and Dissociated Gases", General Electric Co., M.S.V.D., TIS R59SD457, Nov. 1959.
37. Snow, C.W., Wallace, D.R., Lyon, L.L. and Crocker, G.R. "Reaction of Carbon Blacks with Oxygen", Proceedings of the Third Conference on Carbon, Pergamon Press, 1959. pp. 279-287.
38. Grozdovskii and Chukhanov Zhur. Priklad. Khim, Vol. 8, 1934, p. 1398.
39. Tu, C.M., Davies, H., and Hottel, H.C., Ind. Eng. Chem. Vol. 26, p. 749.
40. Davis, H., and Hottel, H.C., Ind. Eng. Chem. Vol. 26, 1934, p. 889.
41. Tsukhanova, O.A., "Solving Problems of Heterogeneous Combustion by the Method of Averaging Equations", Sixth Symposium on Combustion, Rheinhold Publication Corp., New York, 1956, pp. 573-577.
42. Gulbransen, E.A. "Mechanism of the Oxidation of Graphite at Temperatures of 425°C to 575°C.

43. Kuchta, J. M. et al, Ind. Eng. Chem. Vol. 43, 1951, p. 43.
44. Riley, H. L., Chem. and Ind. Vol. 36, 1948, p. 569.
45. Smith, F. W. "Predicted Combustion Characteristics of Brush Carbon Spheres in High Velocity Air", M.I.T. Meteor Report No. 6, Jan. 1957.
46. Winslow, F.H. and Matreyek, W., J. Polymer Sci., Vol. 22, 1956, p. 315.
47. Winslow, F.H. and Baker, W.V., Pape N.K. and Matreyek, W., J. Polymer Sci. Vol. 16, 1955, p. 101.
48. Akamatsu, H., Inokuchi, H., Tokahashi, H., and Matsugu, V., Bull. Chem. Soc. (Japan) Vol. 29, 1956, p. 574.
49. Wicke, E., "Contributions to the Combustion Mechanism of Carbon", Fifth Symposium on Combustion, Reinhold Publishing Co., 1955, pp. 245-252.
50. Hedden, K. and Wicke, E. "About Some Influences on the Reactivity of Carbons", Proceedings of the Third Conference on Carbon, Pergamon Press, 1959, pp. 249-256.
51. Arthur, J.R., BCURA, Vol. 8, 1944, p. 296.
52. Arthur, J.R., BCURA, Vol. 13, 1949, p. 297.
53. Yagi, S. and Kunii, D., "Studies on Combustion of Carbon Particles in Flames and Fluidized Beds", Fifth Symposium on Combustion, Rheinhold Publishing Co., 1955, pp. 231-244.
54. Semechkova, A. F., and Frank-Kamenetskii, D. A., "Vosstanovlenie uglekisloti uglem", Zhur. Fiz. Khim., Vol. 14, 1940, pp. 291-304.
55. Klibanova, Z., and Frank-Kamenetskii, D. A., "Ignition of Carbon and Kinetics of its reaction with Oxygen", Acta Phys., Vol. 18, 1943, pp. 387-405.

56. Horton, W.S., "Oxidation Kinetics of Pyrolytic Graphite", General Electric Co., G. E. L. Report No. 60GL218, Jan. 1961.
57. Streznewski, J. and Turkevich, J. "The Reaction of Carbon with Oxygen Atoms", Proceedings of the Third Conference on Carbon, Pergamon Press, 1959, pp. 273-278.
58. Hirschfelder, J.O., Curtiss, C.F., and Bird, R.B., "Molecular Theory of Gases and Liquids", John Wiley, 1954.
59. Eggers, A. J. Jr., Hansen, C. F. and Cunningham, B. E., "Stagnation - Point Heat Transfer to Blunt Shapes in Hypersonic Flight Including Effects of Yaw", NACA TN 4229, April 1958.

## LIST OF TABLES

- Table I. Oxidation Rates of High Temperature Materials
- Table II. Equilibrium Constants
- Table III. Specific Reaction Rates of Carbonaceous Materials
- Table IV. Gas Constants
- Table V. Thermal Properties of High Temperature Materials

TABLE I. OXIDATION RATES OF HIGH TEMPERATURE MATERIALS AT ATMOSPHERIC PRESSURE, (LB/FT<sup>2</sup>HR)

Material	Melting Point (°R)	T = 1500°R	2000°R	3000°R	4000°R	Ref.
Graphite (fast rate)	7100 (a)	$2.88 \times 10^0$	$2.25 \times 10^1$	$2.25 \times 10^1$	$2.25 \times 10^1$	e
Graphite (slow rate)	7100 (a)	$2.13 \times 10^{-3}$	$8.90 \times 10^{-1}$	$1.98 \times 10^1$	$2.25 \times 10^1$	-
Tungsten	6630 (b)	$2.05 \times 10^{-4}$	$2.05 \times 10^{-2}$	$2.46 \times 10^0$ (*)		b
Tantalum	5884 (b)	$5.12 \times 10^{-4}$ (*)				b
Molybdenum	5189 (b)	$0.15 \times 10^{-1}$ (*)				b
Columbium	4838 (b)	$4.10 \times 10^{-2}$ (*)				b
Hafnium	4046 (b)	$1.23 \times 10^{-3}$ (*)				b
Zirconium	3870 (c)	$9.87 \times 10^{-5}$	$6.63 \times 10^{-4}$ (*)			d
Iron	3260 (c)	$6.66 \times 10^{-4}$ (*)				e
Nickel	3110 (c)	$1.76 \times 10^{-4}$	$5.52 \times 10^{-3}$	$1.76 \times 10^{-1}$ (*)		f
Beryllium	2800 (c)	$2.44 \times 10^{-6}$	$1.22 \times 10^{-5}$			g

(\*) extrapolated

References - Table I

- a) Handbook of Chemistry and Physics, 40th Ed., Chem. Rubber Co., Ohio, 1958
- b) R. I. Jaffe, "Refractory Metals", Battelle Memorial Institute, Presented at Symposium on High Temperature Technology, Stanford Research Inst., Calif., Oct. 1959
- c) W. G. Bradshaw and C. O. Matthews, "Properties of Refractory Materials: Collected Data and References", Lockheed Report # LMSD-2466, Jan. 1959
- d) R. G. Charles, S. Barnartt, E. A. Gulbransen, "Prolonged Oxidation of Zirconium at 350 and 450°C", Trans. of Metallurgical Soc. of AIME., Vol. 212, No. 1, p. 101, Feb. 1958
- e) J. W. Evans and S. K. Chatterji, "Influence of Silicon on the High Temperature oxidation of Copper and Iron", J. Electrochemical Soc., Vol. 106, No. 10, Oct. 1959
- f) G. E. Zima, "Some High Temperature Oxidation Characteristics of Nickel with Chromium Additions", Trans. of American Society for Metals, Vol. 49, 1957, pp. 924-947
- g) E. A. Gulbransen and K. F. Andrew, J. Electrochem. Soc. 97, 383-395, 1950

TABLE II. EQUILIBRIUM CONSTANTS,  $\log_{10} K_p = a - b/T(^{\circ}R)$

Reaction	Equilibrium Constant $K_p$ is in atm.	a	$b \times 10^{-4}$
$O_2 \rightleftharpoons 2O$	$K_{pO} = (P_O)^2 / P_{O_2}$	6.86	4.68
$N_2 \rightleftharpoons 2N$	$K_{pN} = (P_N)^2 / P_{N_2}$	7.00	9.00
$2CO \rightleftharpoons CO_2 + C(s)$	$K_{pCO_2} = P_{CO_2} / (P_{CO})^2$	-8.80	-1.503
$CO + O \rightleftharpoons CO_2$	$K_{pCO} = P_{CO_2} / P_{CO} \cdot P_O$	-8.00	5.04
$C(s) \rightleftharpoons C(g)$	$K_{pC} = P_C$	8.17	6.72
$2C(s) \rightleftharpoons C_2(g)$	$K_{pC_2} = P_{C_2}$	9.71	7.63
$3C(s) \rightleftharpoons C_3(g)$	$K_{pC_3} = P_{C_3}$	9.83	7.26
$NO \rightleftharpoons N + O$	$K_{pNO} = P_N \cdot P_O / P_{NO}$	6.39	6.06
$C(s) + 1/2N_2 \rightleftharpoons CN$	$K_{pCN} = P_{CN} / (P_{N_2})^{1/2}$	5.00	3.60

Based on data appearing in:

B. Lewis and G. von Elbe, "Combustion, Flames and Explosions of Gases",  
Academic Press, New York, 1951

Table III. SPECIFIC REACTION RATES OF CARBONACEOUS MATERIALS

Investigator	Rate Law	E, F cal./mole	C. G. S.	F. P. S.
Parker & Hottel (Ref. 20)	$\dot{m}_w = k P_{O_2}$	44.0	$9.550 \times 10^6 \frac{\mu\text{m}(\text{K})^{1/2}}{\text{cm}^2 \cdot \text{sec}(\text{Atm})}$	$2.025 \times 10^7 \frac{\text{Lb}(\text{R})^{1/2}}{\text{Ft}^2 \cdot \text{sec}(\text{Atm})}$
Gulbransen & Andrew (Ref. 21)	$\dot{m}_w = k$	30.7	$1.193 \times 10^2 \mu\text{m}/\text{cm}^2 \cdot \text{sec.}$	$2.443 \times 10^2 \text{ Lb}/\text{Ft}^2 \cdot \text{sec.}$
Frank & Kamenetskii (Ref. 6)	$\dot{m}_w = k (P_{O_2})^{1/2}$ ( $T_0 = 1800^\circ \text{R}$ )	44.0	$1.049 \times 10^{-3} \frac{\mu\text{m}(\text{K})^{1/2}}{\text{cm}^2 \cdot \text{sec}(\text{Atm})^{1/2}}$	$2.883 \times 10^{-3} \frac{\text{Lb}(\text{R})^{1/2}}{\text{Ft}^2 \cdot \text{sec}(\text{Atm})^{1/2}}$
Vulis (Ref. 23)	$\dot{m}_w = k P_{O_2}$ ( $T^* = 2232^\circ \text{R}$ )	17.72	$1.233 \times 10^1 \frac{\mu\text{m} \cdot \text{K}}{\text{cm}^2 \cdot \text{sec} \cdot \text{Atm.}}$	$4.547 \times 10^1 \frac{\text{Lb} \cdot \text{R}}{\text{Ft}^2 \cdot \text{sec} \cdot (\text{Atm})}$
Blyholder & Eyring (Ref. 22)	$\dot{m}_w = k$	42.3	$1.228 \times 10^2 \mu\text{m}/\text{cm}^2 \cdot \text{sec.}$	$2.515 \times 10^2 \text{ Lb}/\text{Ft}^2 \cdot \text{sec.}$

@  $P_{O_2} = 2 \text{ Atm}$

R = 1.987 cal./mole °K = 1.104 cal./mole °R

TABLE IV. GAS CONSTANTS (\*T<sub>ref</sub> = 536.7°R)

Species	$\sigma_1^{\circ}, \text{\AA}$	$M_1$	$\epsilon/\text{\AA}^{\circ}\text{K}$	$\omega_e, \text{cm}^{-1}$	$\Delta h_f^{\circ} (*), \text{BTU/LB}$
O	2.960 (a)	16	—	—	6,654 (f)
O <sub>2</sub>	3.541 (b)	32	88.0 (a)	1580.4 (d)	0
N	2.880 (a)	14	—	—	14,527 (e)
N <sub>2</sub>	3.749 (b)	28	79.8 (b)	2359.5 (d)	0
CO	3.590 (c)	28	110.0 (c)	2156.7 (d)	-1,698 (f)
CO <sub>2</sub>	3.897 (b)	44	213.0 (b)	2349, 1388, 667 (2) (d)	-3,848 (f)

57

- a) Hirschfelder, J. and Eliason, M., "The Estimation of Transport Properties for Electronically Excited Atoms and Molecules", Technical Report Wis-AF-1; Contract AF 33(616) 3414, May 14, 1956
- b) Trautz, M., Melster, A., and Zink, R., Ann. Physik, Vol. 5, No. 7, 1930, pp. 409 - 452
- c) Johnston, H. and McCloskey, K., J. Phys. Chem., Vol. 44, p. 1038, 1940
- d) Herzberg, G., "Spectra of Diatomic Molecules", Van Nostrand Co., Inc., New York, 1950
- e) Kistiakowsky, G., Knight, H., and Malin, M., Gaseous Deionations III Dissociation Energies of N<sub>2</sub> and CO", J. Chem. Phys., Vol. 20, May 1952, p. 876
- f) Gordon, J., "Thermodynamics of High Temperature Gas Mixtures, and Application to Combustion Problems", WADC Tech. Report 57-33, ASTIA Document No. 110735, January 1957

TABLE V. THERMAL PROPERTIES OF HIGH TEMPERATURE MATERIALS

Material	Density LB/FT <sup>3</sup>	Thermal Conductivity (*) BTU - FT/LT <sup>2</sup> HR <sup>2</sup> R	Specific Heat (*) BTU/LB <sup>2</sup> R	Thermal Diffusivity (**) FT <sup>2</sup> /HR.	Total Emissivity
Graphite (**)	96.1 - 117.4	(H) 64.6 - 91.2 (L) 52.5 - 66.3	0.173	(H) 3.18 - 5.49 (L) 4.78 - 3.99	.75 - .85
Tungsten (b)	1205	116.2	0.032	3.01	.10 - .40 (c)
Tantalum (b)	1355	31.5	0.031	0.981	.19 - .31 (c)
Molybdeum (b)	636.8	84.7	0.051	2.18	.10 - .25 (c)
Columbium (b)	534.4	33.2	0.055	0.869	.19 - .23 (d)
Hafnium (b)	834.1	12.8	0.035	0.439	—

- (\*) Values taken at room temperature  
 (\*\*) Petroleum coke-based graphites.  
 (H) Parallel to grain  
 (L) Perpendicular to grain

References

- (a) The Industrial Graphite Engineering Handbook, National Carbon Co., 1959  
 (b) R. I. Jaffe, "Refractory Metals", Battelle Memorial Institute, Presented at High Temperature Technology Symposium, Stanford Research Institute, Calif., 1959  
 (c) J. G. Bradshaw and C. O. Matthews, "Properties of Refractory Materials: Collected Data and References", Lockheed Aircraft Corporation, LMSD - 2486, Jan. 1959  
 (d) Handbook of Chemistry and Physics, 40th Edition, Chemical Rubber Publishing Co., Cleveland, 1958 - 1959

- Figure 1. Coordinate System
- Figure 2. Viscosity Coefficients of Pure Species
- Figure 3. Binary Diffusion Coefficients of Pure Species
- Figure 4. Self-Diffusion Coefficients of Pure Species
- Figure 5. Specific Heat of Pure Species
- Figure 6. Enthalpy of Pure Species
- Figure 7. Density-Viscosity Variation for Graphite Combustion
- Figure 8. Variation of Surface Prandtl Number with Surface Temperature
- Figure 9. Typical Surface Lewis Numbers
- Figure 10. Velocity and Temperature Profiles
- Figure 11. Concentration Profiles for Graphite Combustion
- Figure 12. Reaction Rate Profiles
- Figure 13. Typical Eigenvalues for Graphite Combustion
- Figure 14. Ratio of Oxygen to Nitrogen at the Surface of Burning Graphite

- Figure 15. Reaction Rate Controlled Mass Transfer**
- Figure 16. Mass Fraction Ratio of Combustion Products at Graphite Surface**
- Figure 17. Mass Transfer Comparison for a Typical Flight Condition**
- Figure 18. Mass Transfer for Graphite Combustion**
- Figure 19. Mass Transfer Transition Curves for Graphite Combustion**
- Figure 20. Mass Transfer Regimes for Ablating Graphite**
- Figure 21. Typical Heat Transfer into Solid Graphite**
- Figure 22. Comparison of Modes of Energy Transfer to a Burning Graphite Surface**
- Figure 23. Heat Transfer Correlation for Heat Conducted into Solid Graphite**
- Figure 24. Correlated Heat Transfer into Solid Graphite versus Surface Temperature**
- Figure 25. The Effective Heat of Ablation for Graphite in the Diffusion Controlled Oxidation Regime**
- Figure 26. Shear Function for a Typical Flight Condition**
- Figure 27. Correlated Skin Friction Coefficient**
- Figure 28. Axially-Symmetric Stagnation Point Radiation Equilibrium Surface Temperature**

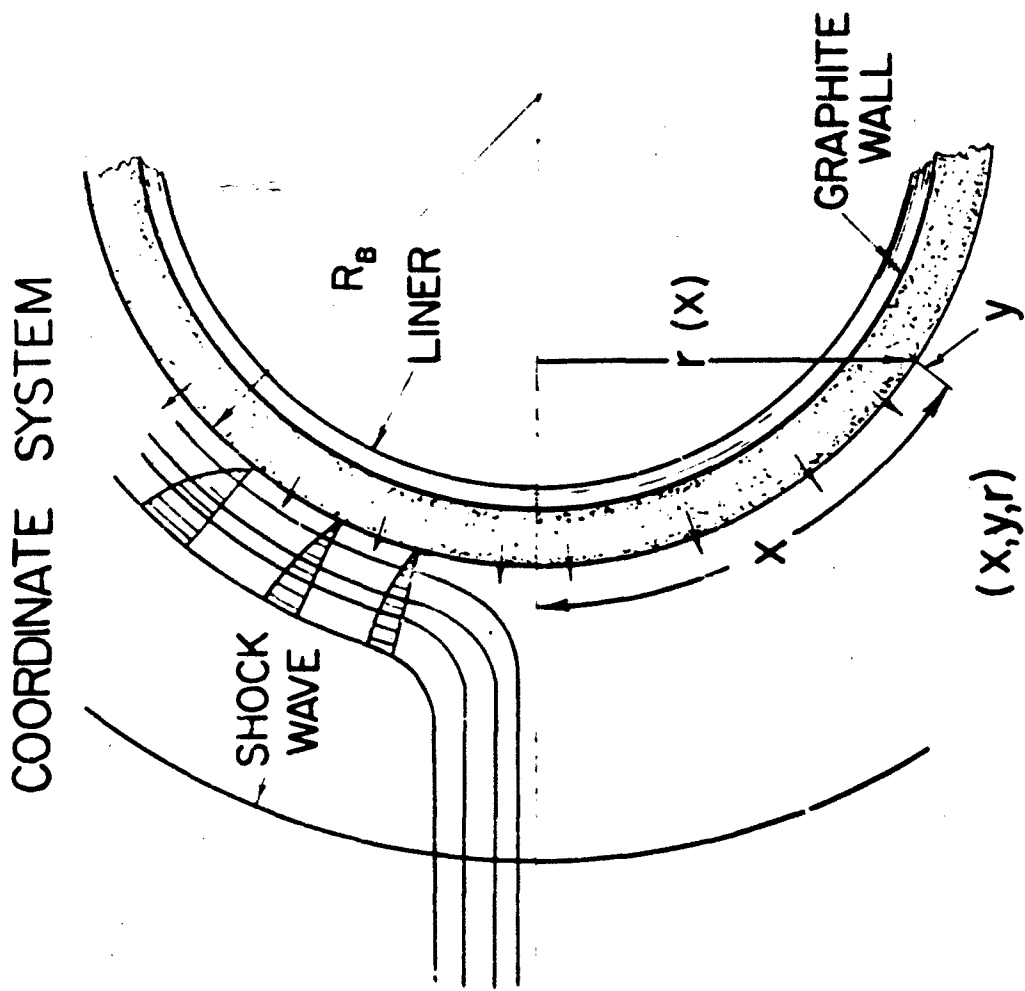


FIGURE 1

# VISCOSITY COEFFICIENTS OF PURE SPECIES

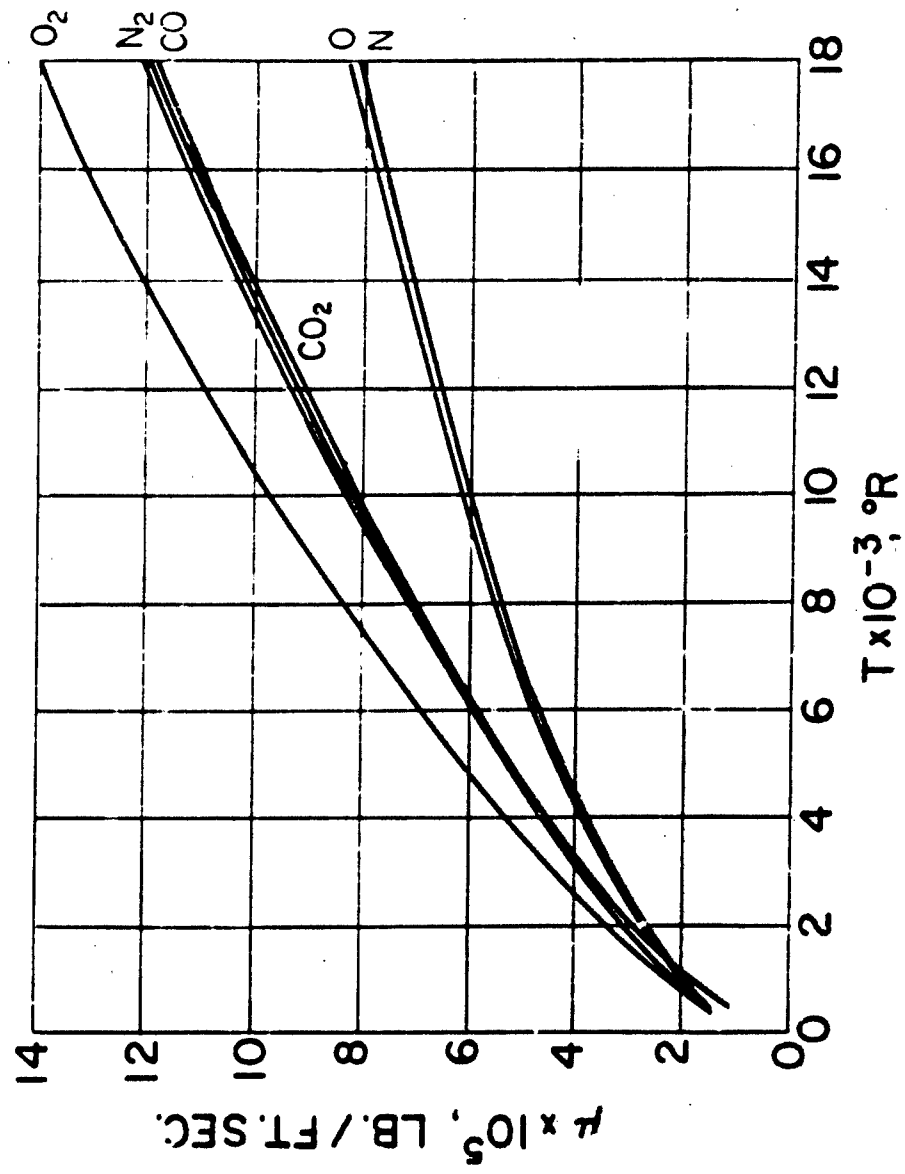


FIGURE 2

# BINARY DIFFUSION COEFFICIENTS OF PURE SPECIES

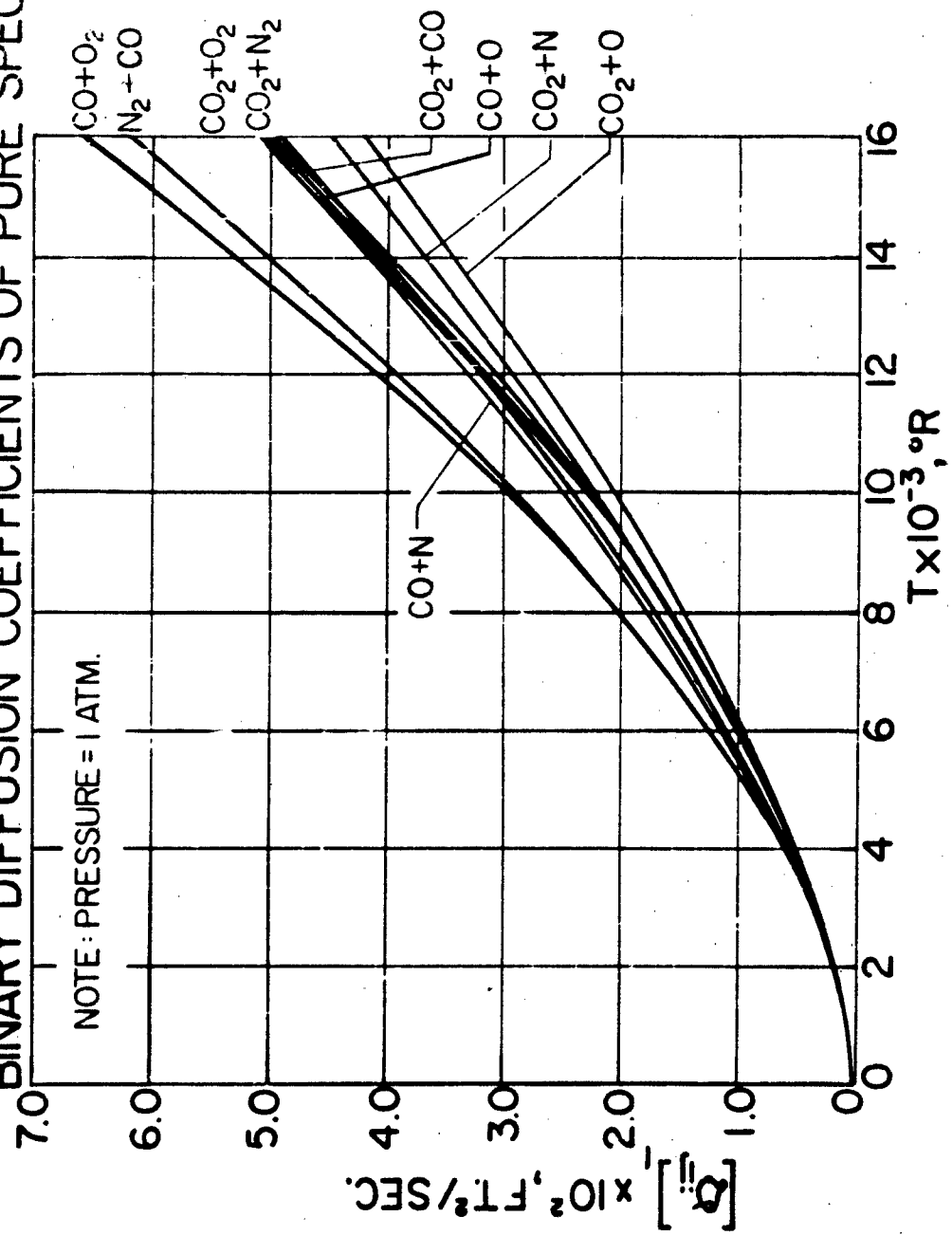


FIGURE 3

# SELF DIFFUSION COEFFICIENTS OF PURE SPECIES

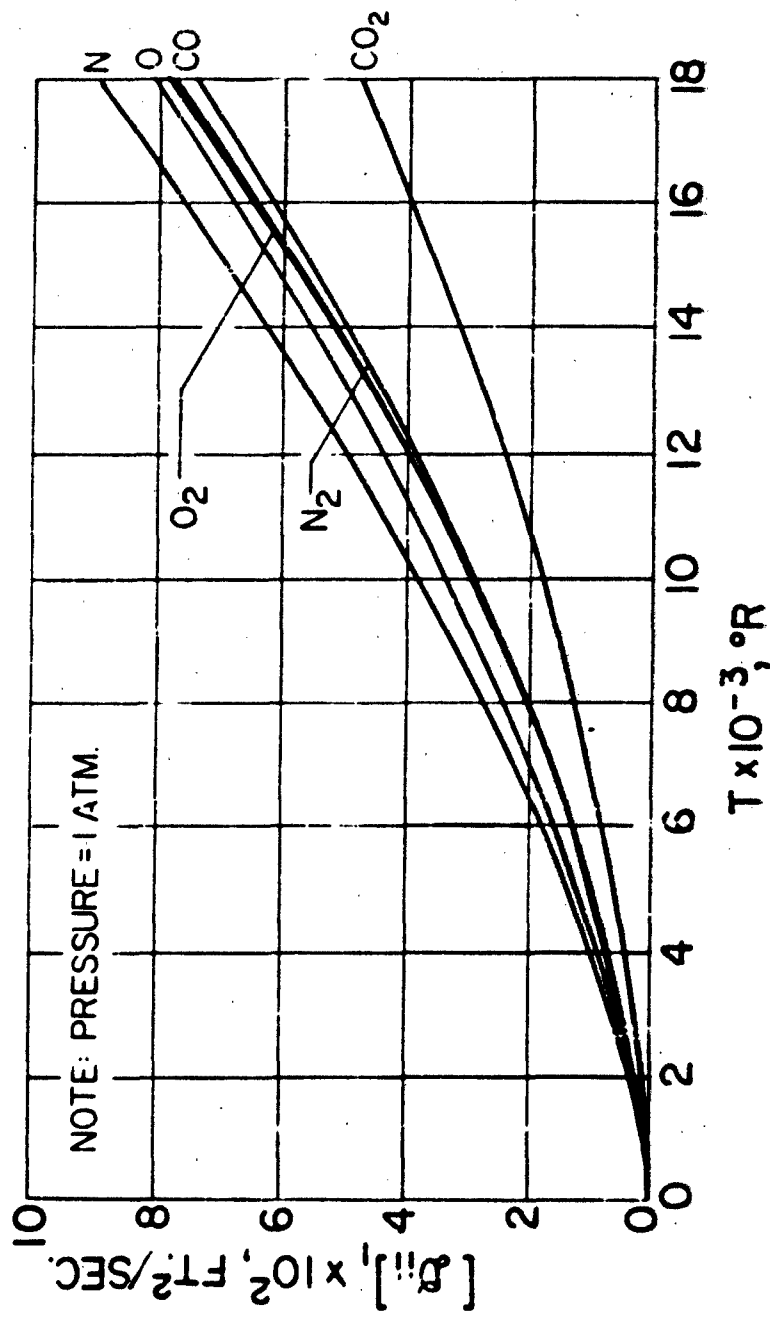


FIGURE 4

# SPECIFIC HEAT OF PURE SPECIES FOR GRAPHITE COMBUSTION

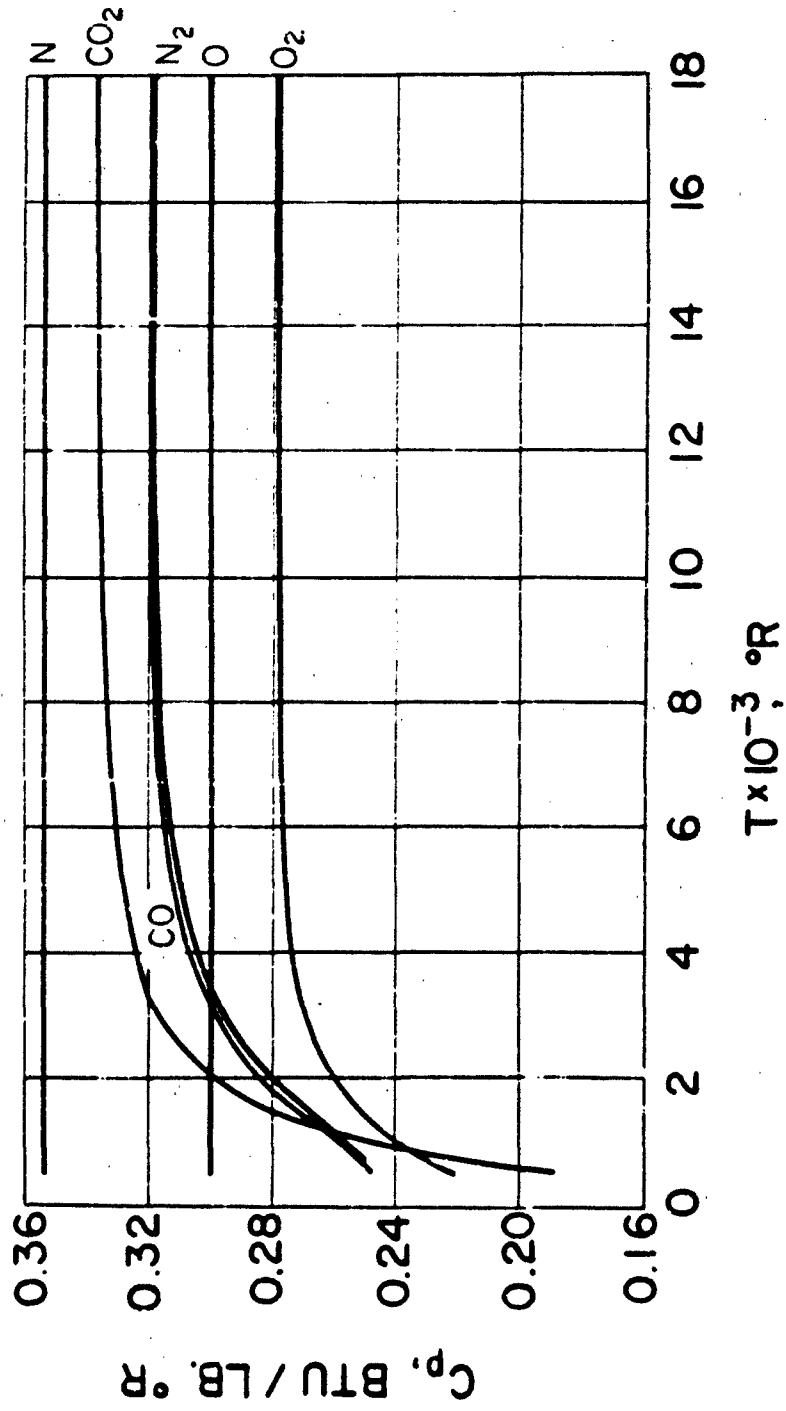


FIGURE 5

# ENTHALPY OF PURE SPECIES FOR GRAPHITE COMBUSTION

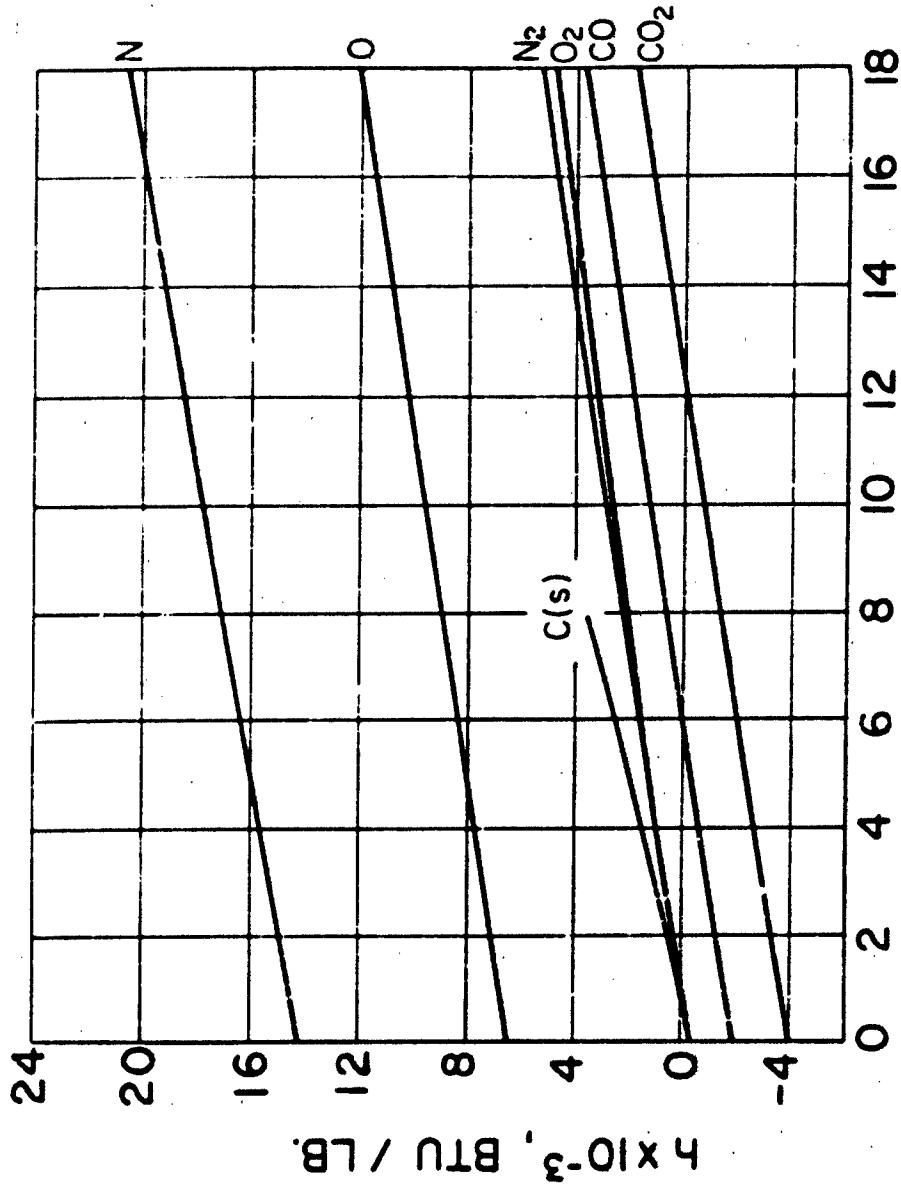


FIGURE 6

# DENSITY-VISCOSITY VARIATION FOR GRAPHITE COMBUSTION

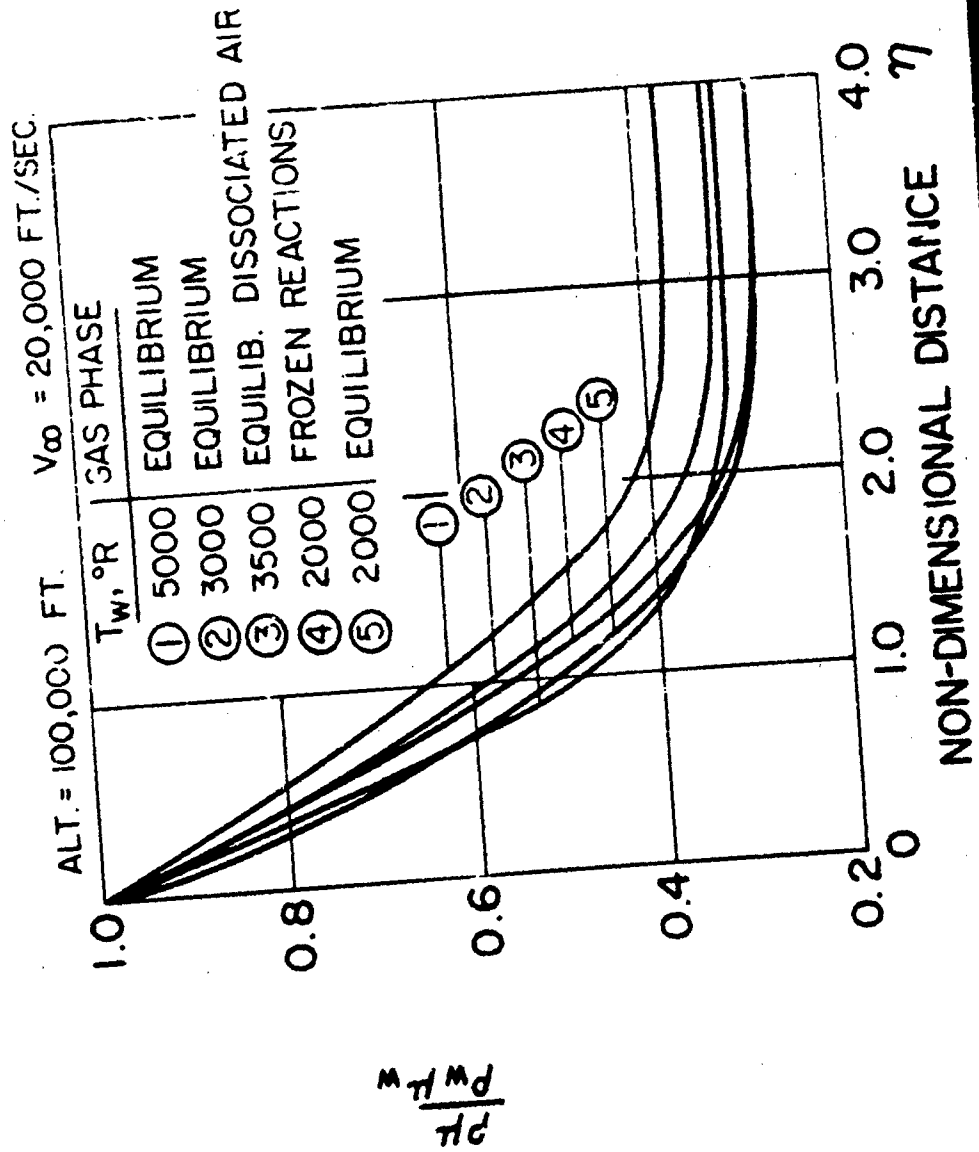


FIGURE 7

VARIATION OF SURFACE PRANDTL NUMBER WITH SURFACE TEMPERATURE

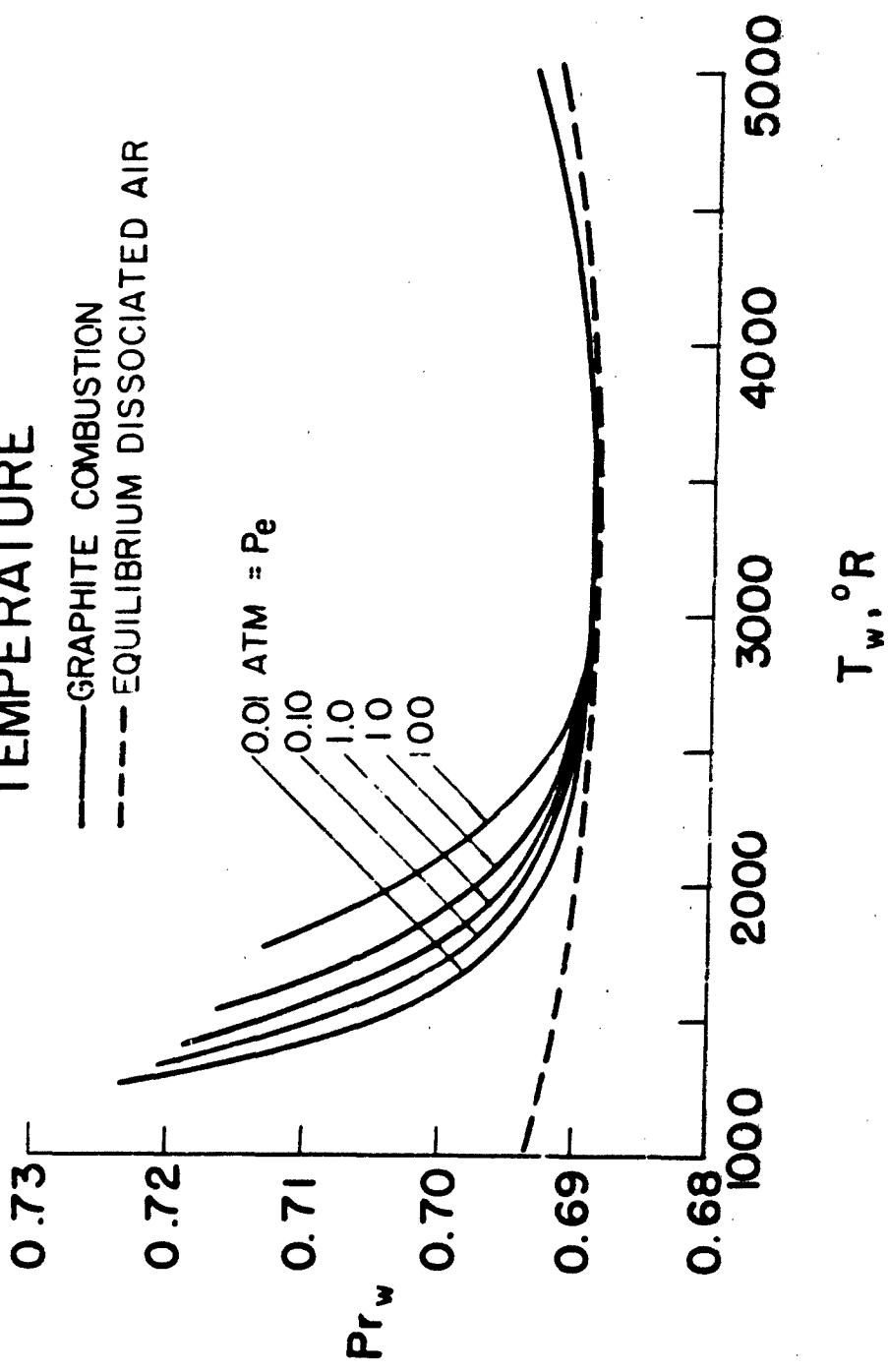


FIGURE 8

# TYPICAL SURFACE LEWIS NUMBERS

(GRAPHITE COMBUSTION)

$P_e = 5.7 \text{ ATM.}$

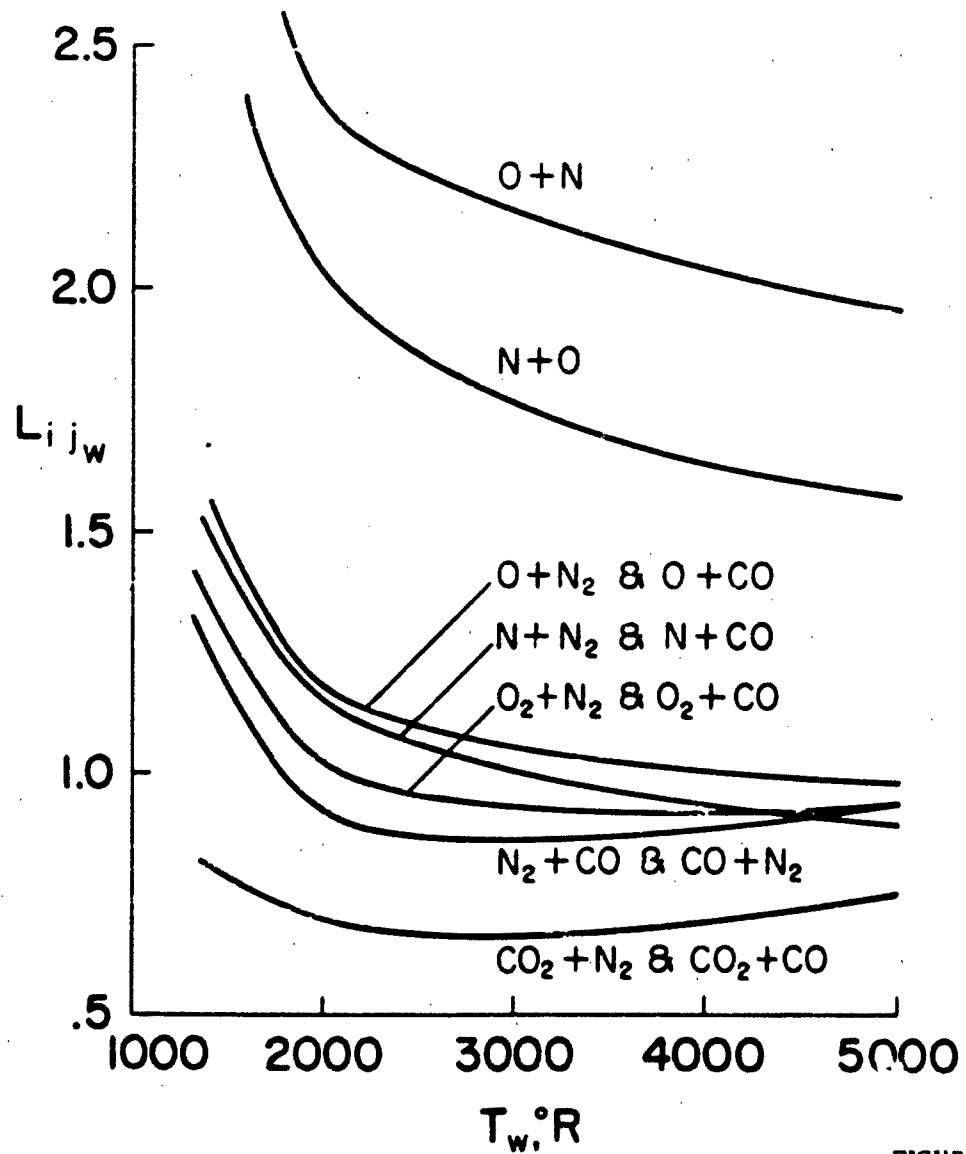


FIGURE 9

# VELOCITY AND TEMPERATURE PROFILES

(GRAPHITE COMBUSTION)

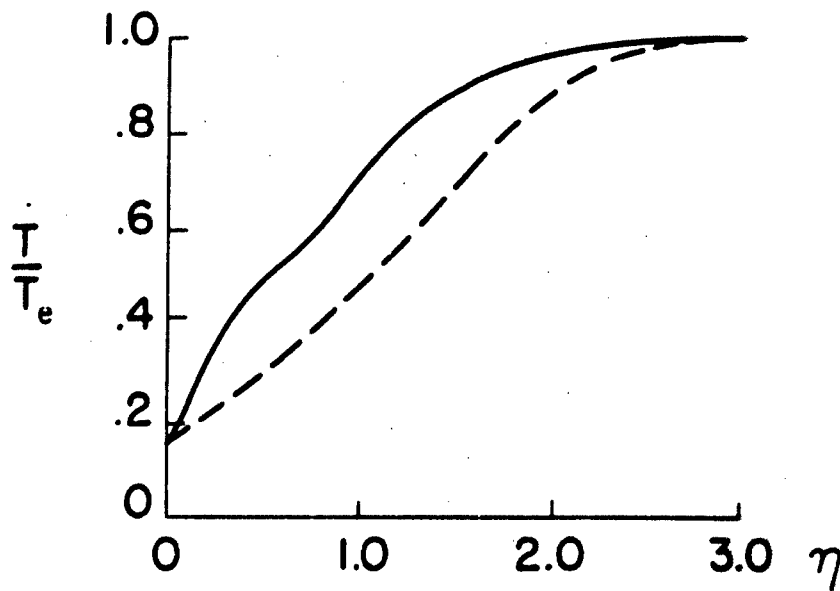
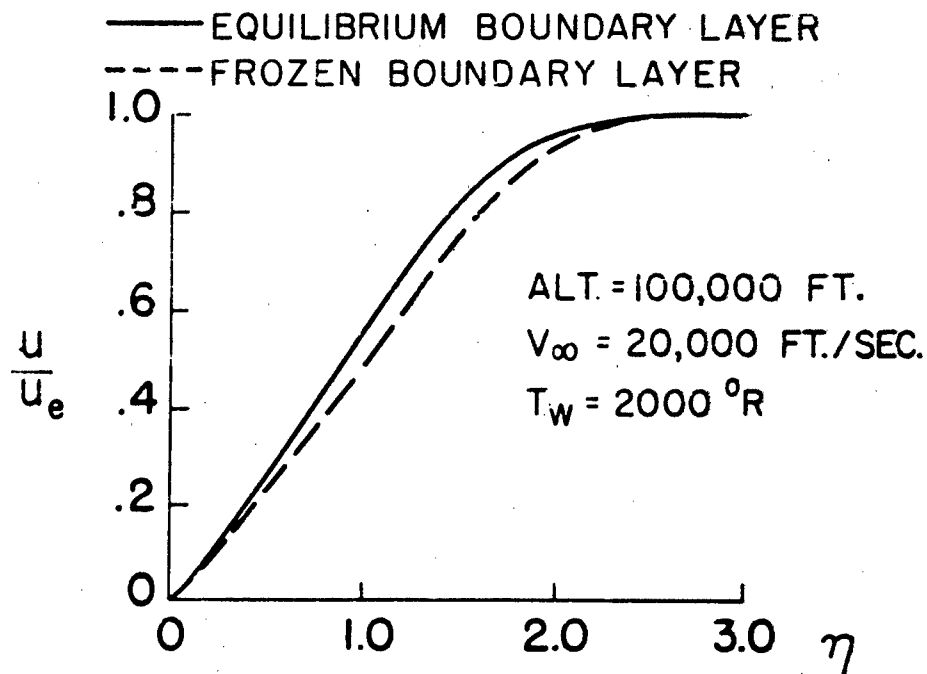


FIGURE 10

# CONCENTRATION PROFILES FOR GRAPHITE COMBUSTION

ALT. = 100,000 FT.;  $V_{\infty} = 20,000$  FT./SEC.;  $T_w = 2000^{\circ}\text{R}$

— EQUILIBRIUM BOUNDARY LAYER  
 - - - FROZEN BOUNDARY LAYER

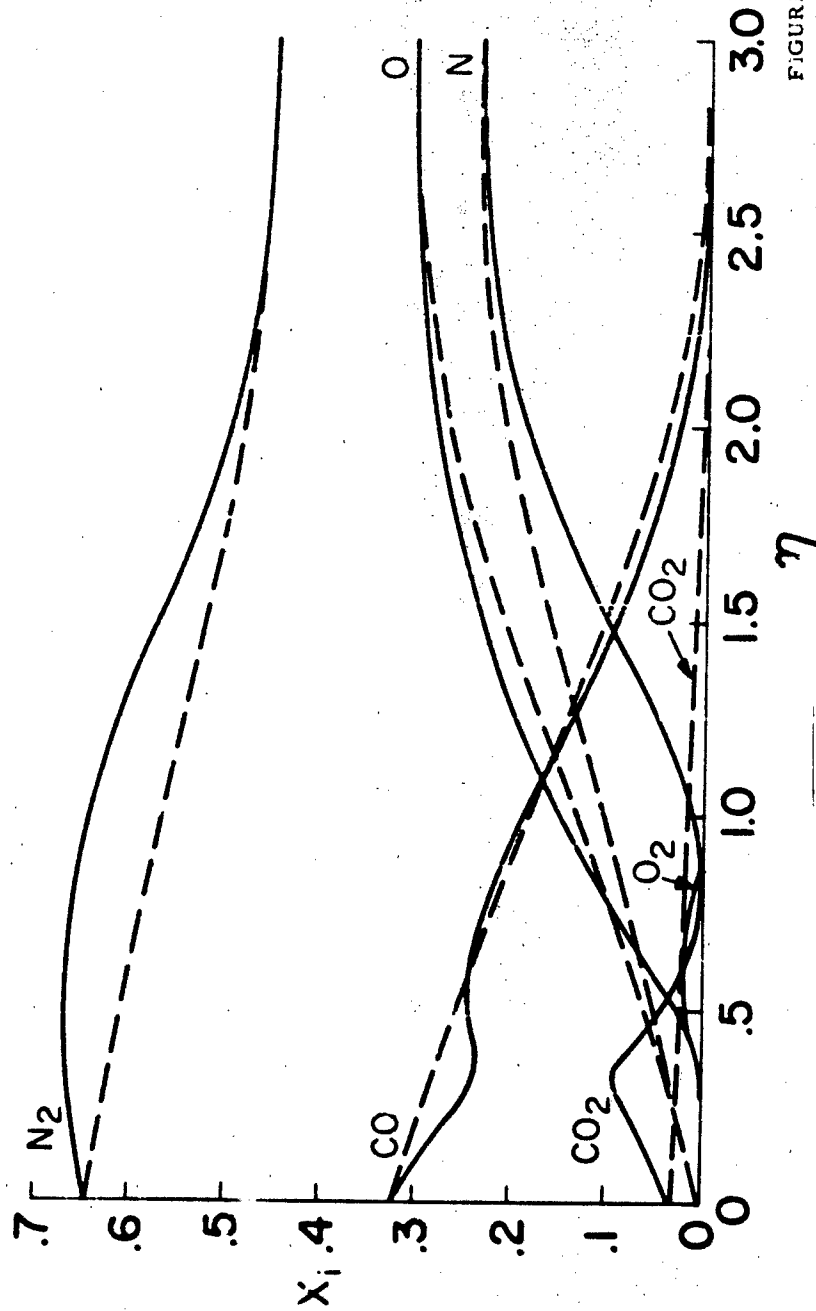
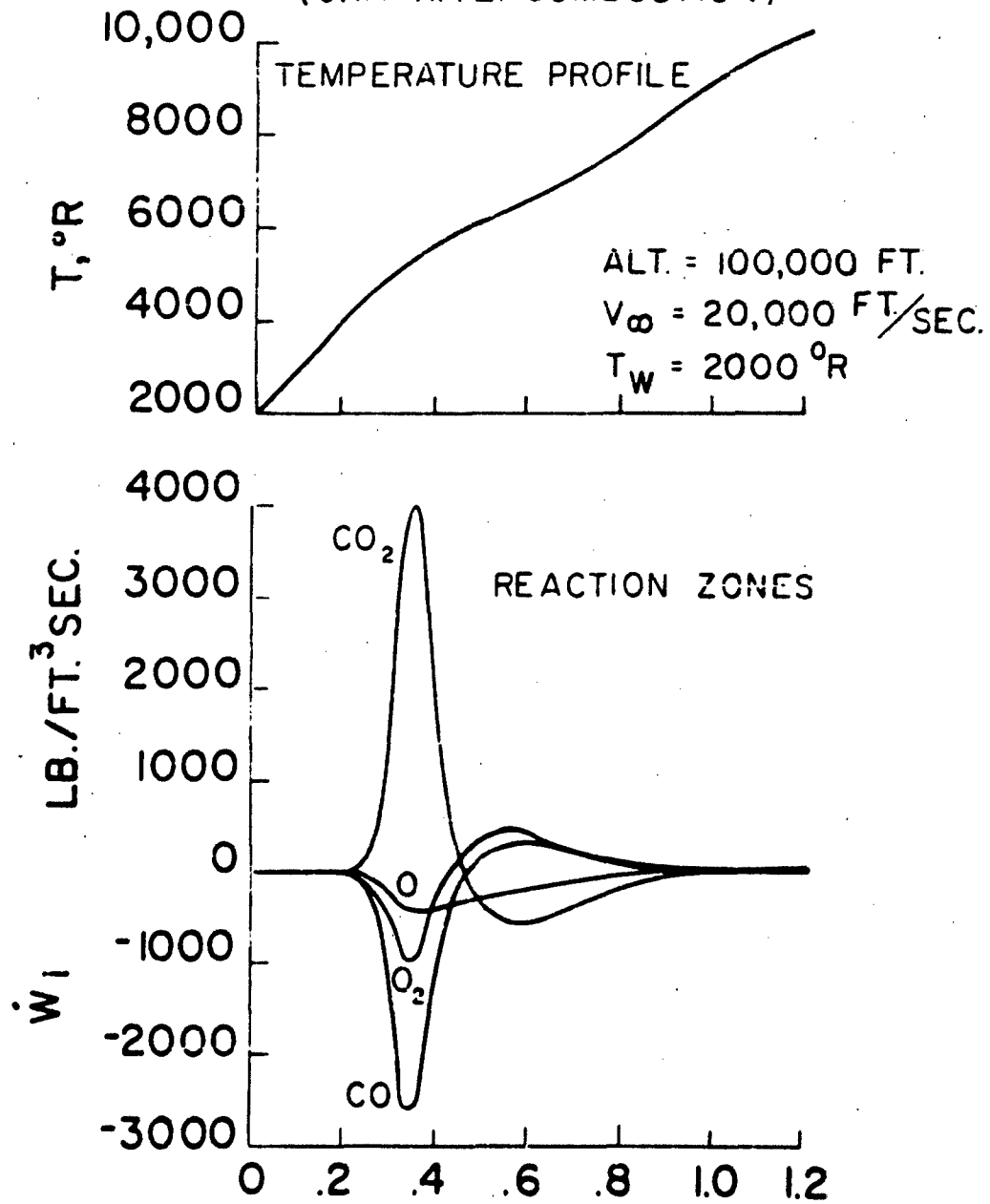


FIGURE 11

# EQUILIBRIUM BOUNDARY LAYER PROFILES

(GRAPHITE COMBUSTION)



$\eta$  FIGURE 12

# TYPICAL EIGENVALUES FOR GRAPHITE COMBUSTION

ALT. = 100,000 FT     $V_{\infty} = 20,000$  FT / SEC.

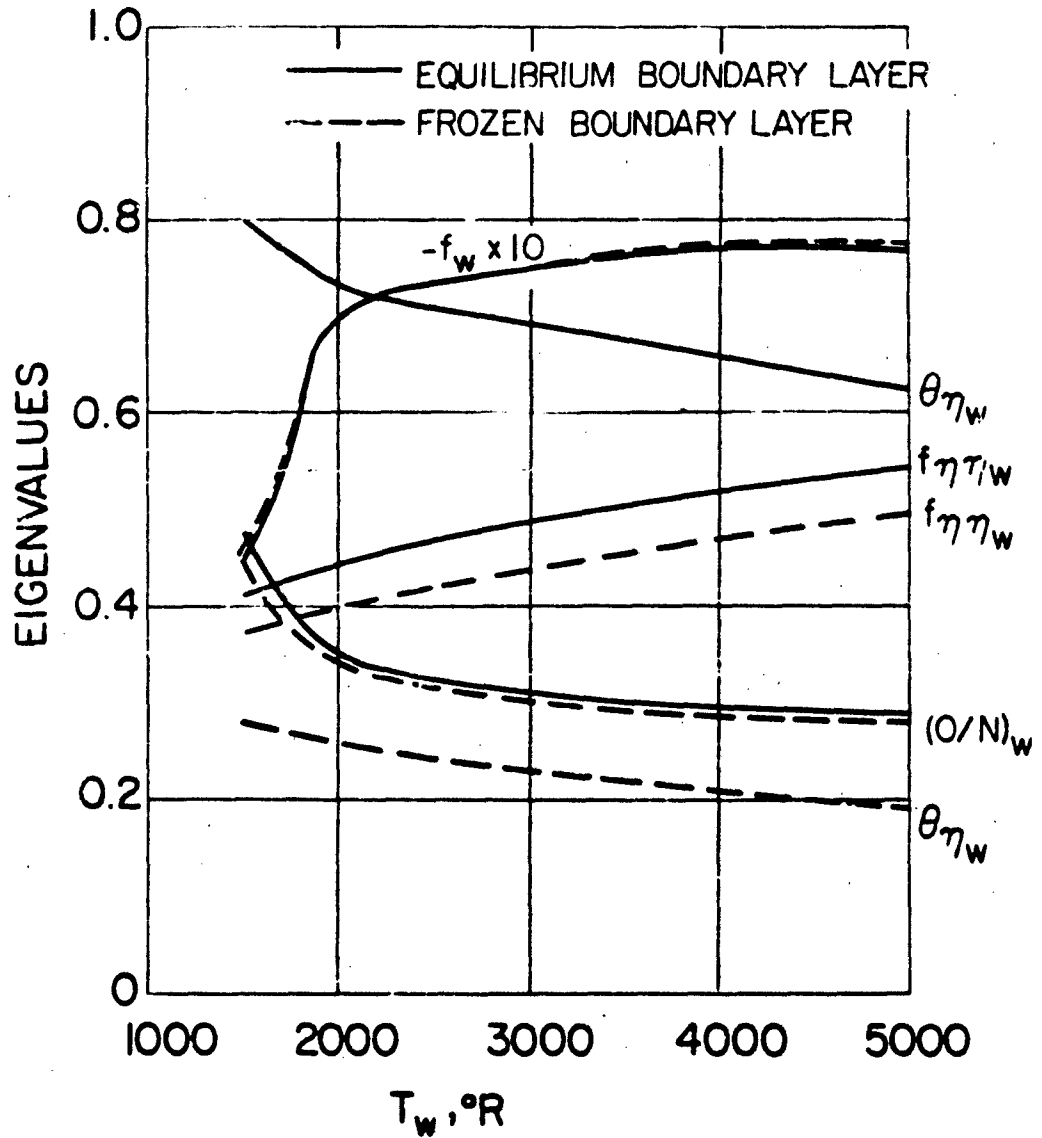


FIGURE 13

# RATIO OF OXYGEN TO NITROGEN AT THE SURFACE OF BURNING GRAPHITE

( DIFFUSION CONTROLLED REGIME )

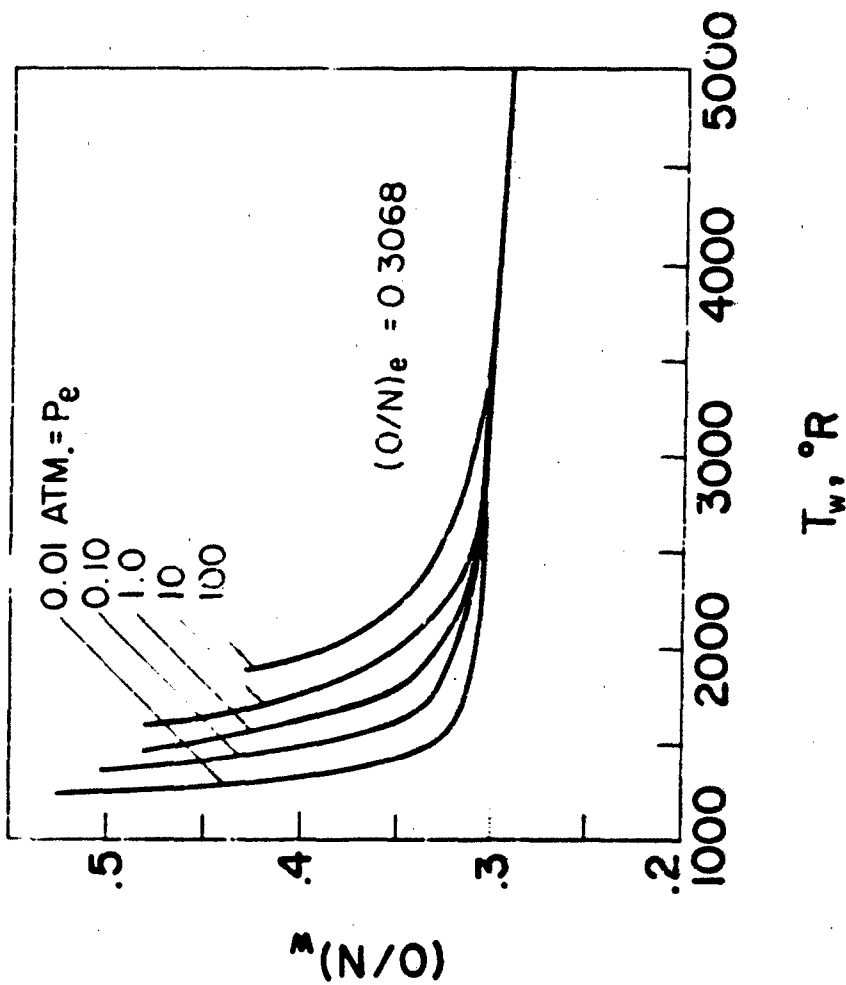


FIGURE 14

# MASS FRACTION RATIO OF COMBUSTION PRODUCTS AT GRAPHITE SURFACE

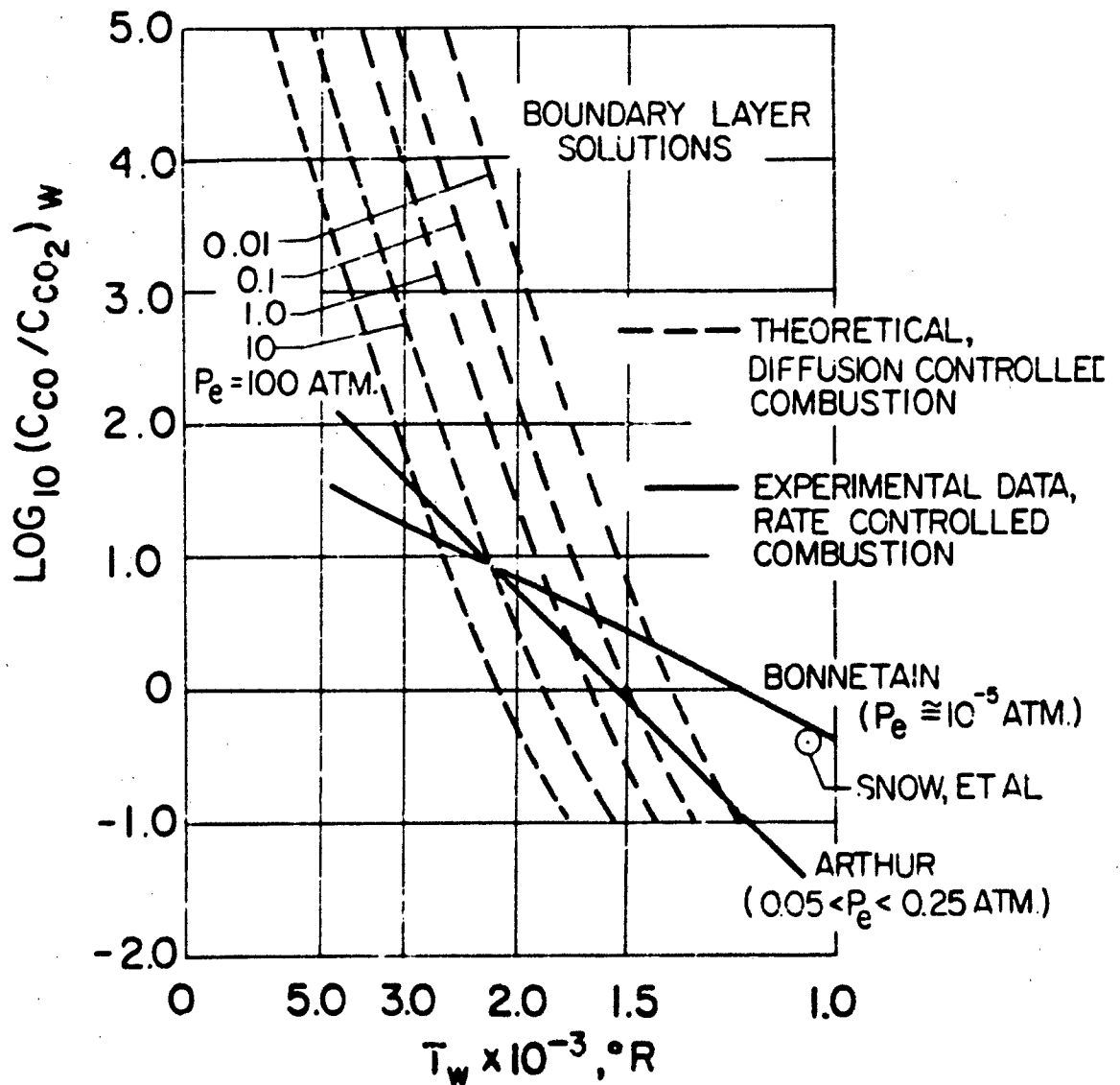


FIGURE 15

# REACTION RATE CONTROLLED MASS TRANSFER

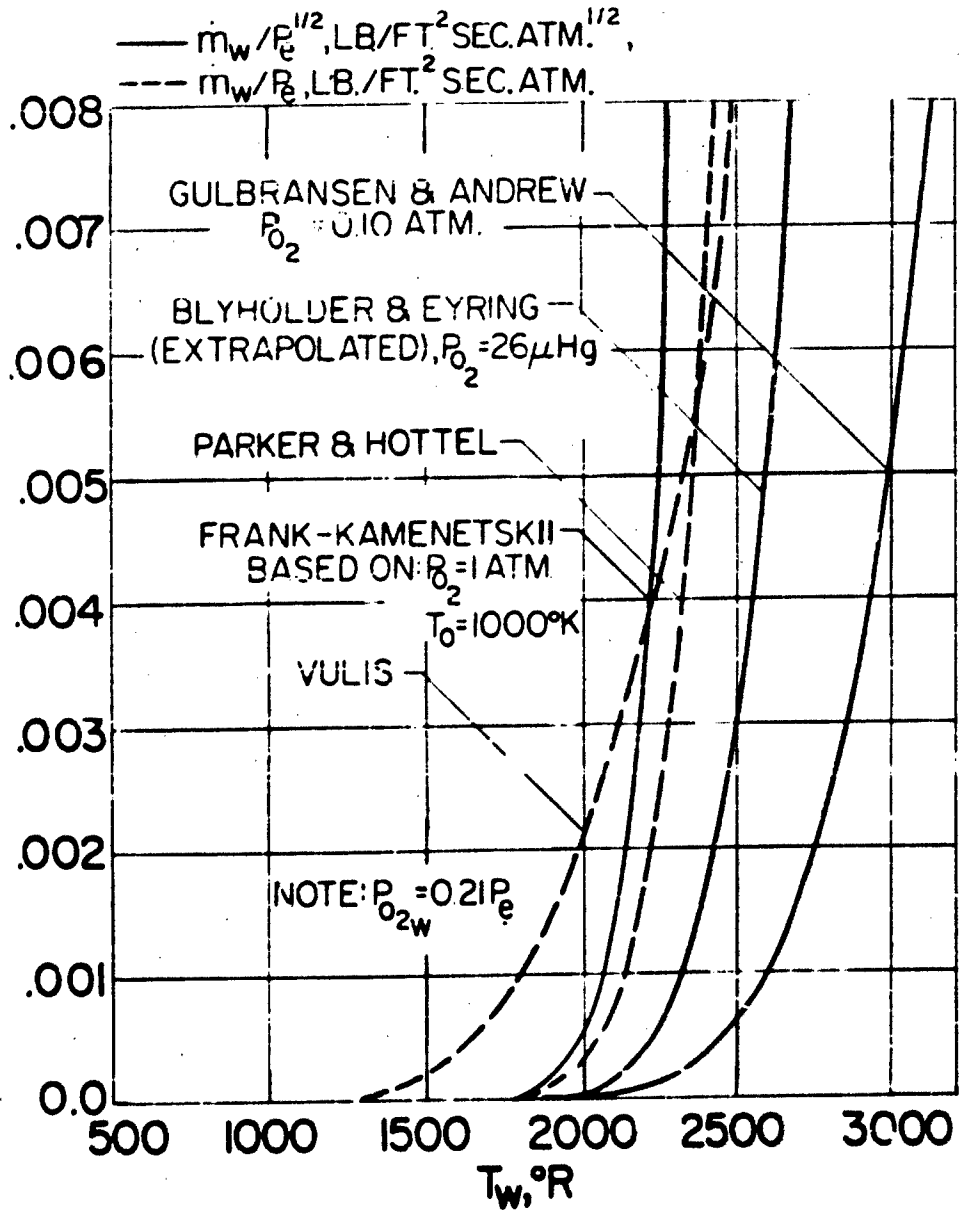


FIGURE 16

# MASS TRANSFER COMPARISON FOR A TYPICAL FLIGHT CONDITION

$$\Delta = 0, \delta = 1$$

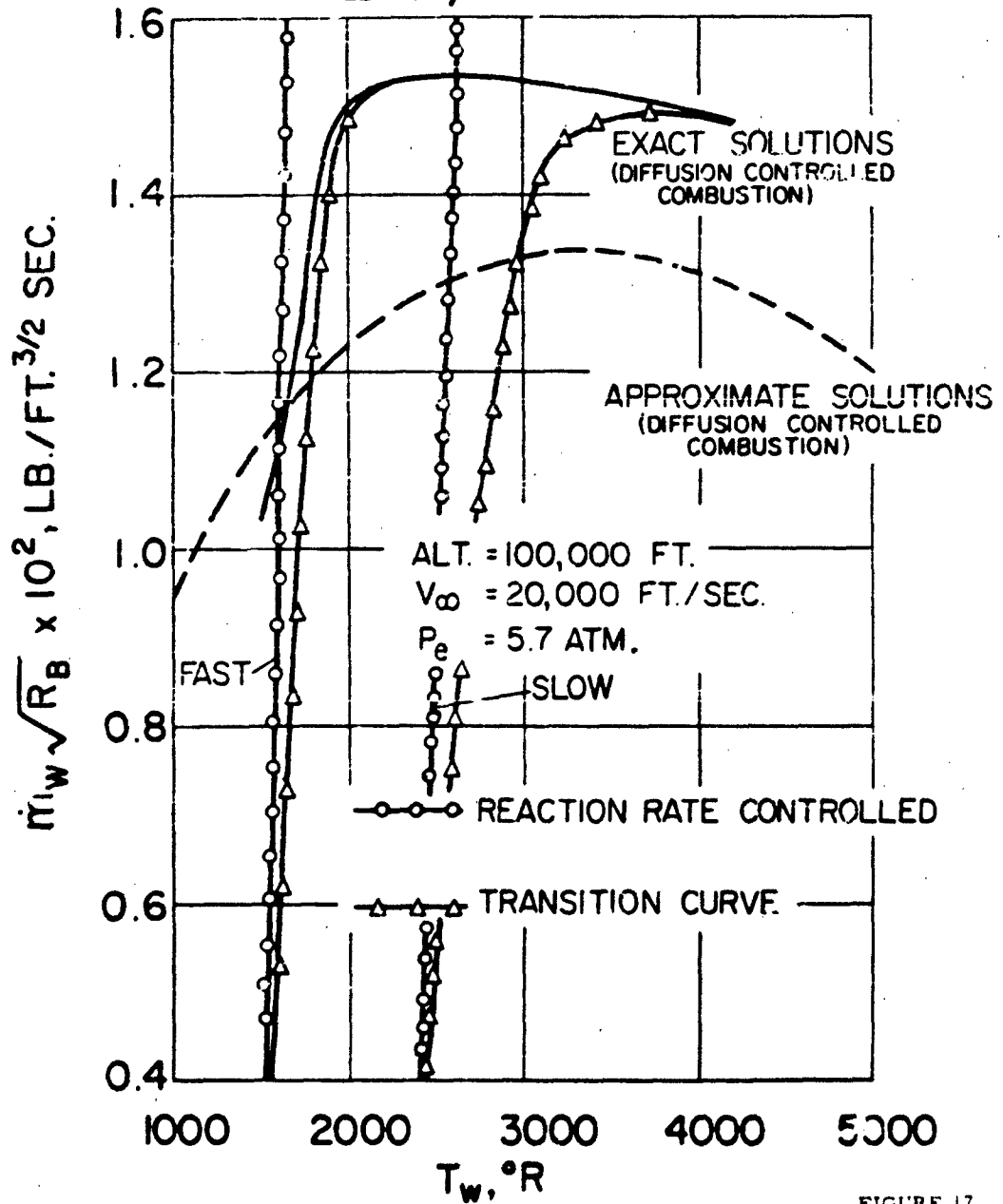


FIGURE 17

# MASS TRANSFER FOR GRAPHITE COMBUSTION

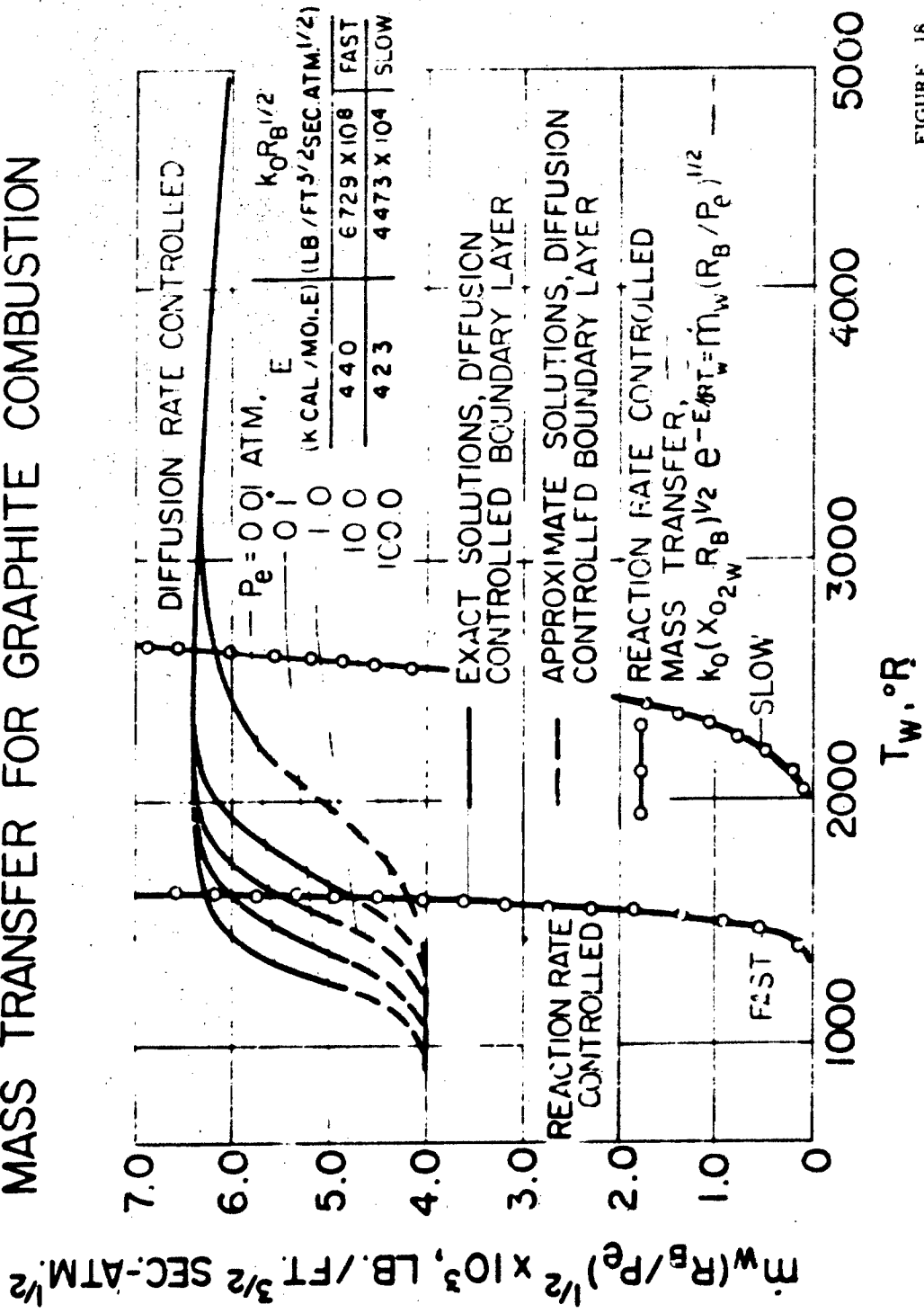


FIGURE 16

# MASS TRANSFER TRANSITION CURVES, GRAPHITE COMBUSTION

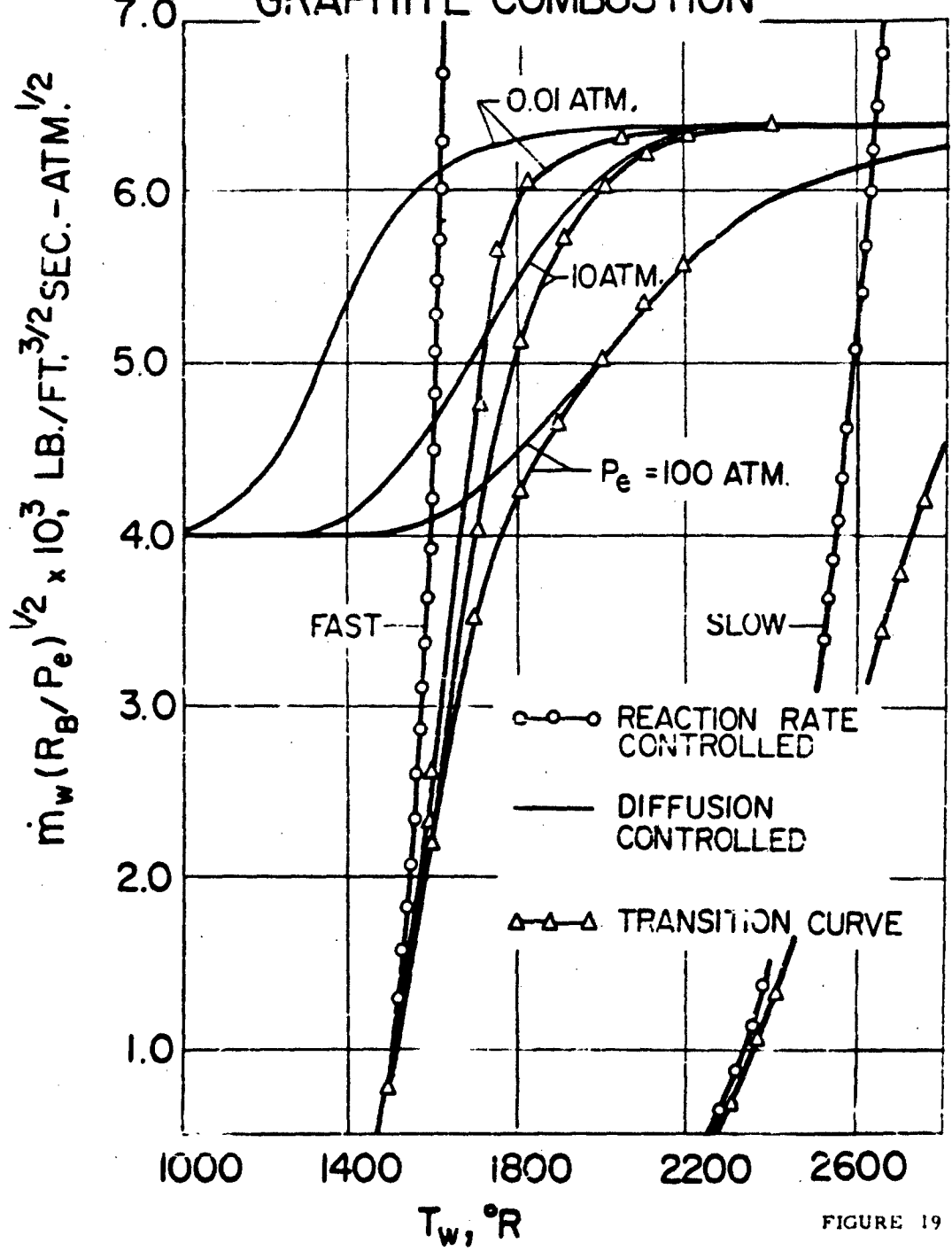


FIGURE 19

# MASS TRANSFER REGIMES FOR ABLATING GRAPHITE

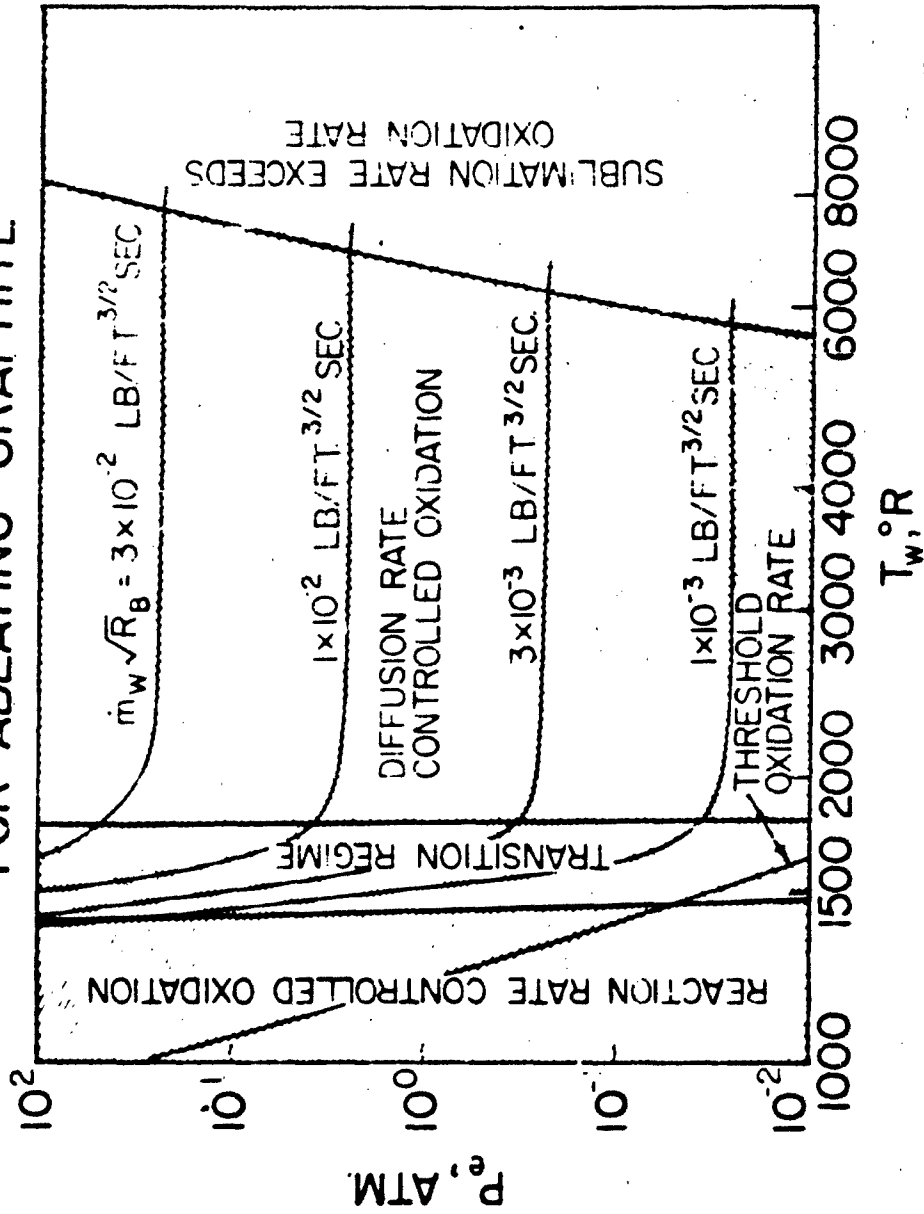


Figure 20

# TYPICAL HEAT TRANSFER INTO SOLID GRAPHITE

ALT. = 100,000 FT.  $V_{\infty} = 20,000$  FT./SEC.

$\Lambda = 0$  ,  $\delta = 1$

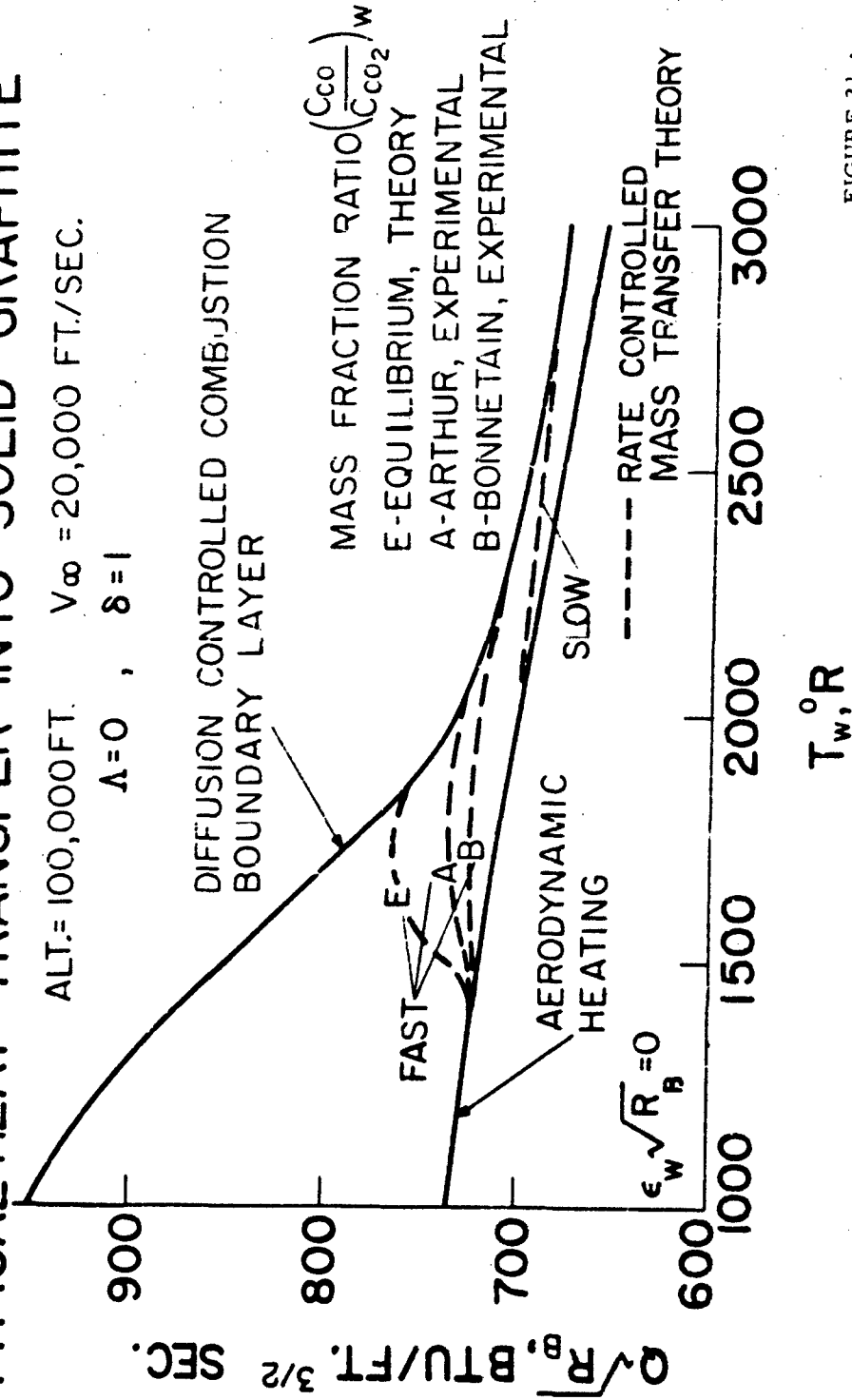


FIGURE 21 •

# COMPARISON OF MODES OF ENERGY TRANSFER TO A BURNING GRAPHITE SURFACE

$$\Lambda = 0, \delta = 1$$

$$\epsilon_w \sqrt{R_B} = 0$$

$$\text{ALT.} = 100,000 \text{ FT.}$$

$$V_\infty = 20,000 \text{ FT./SEC.}$$

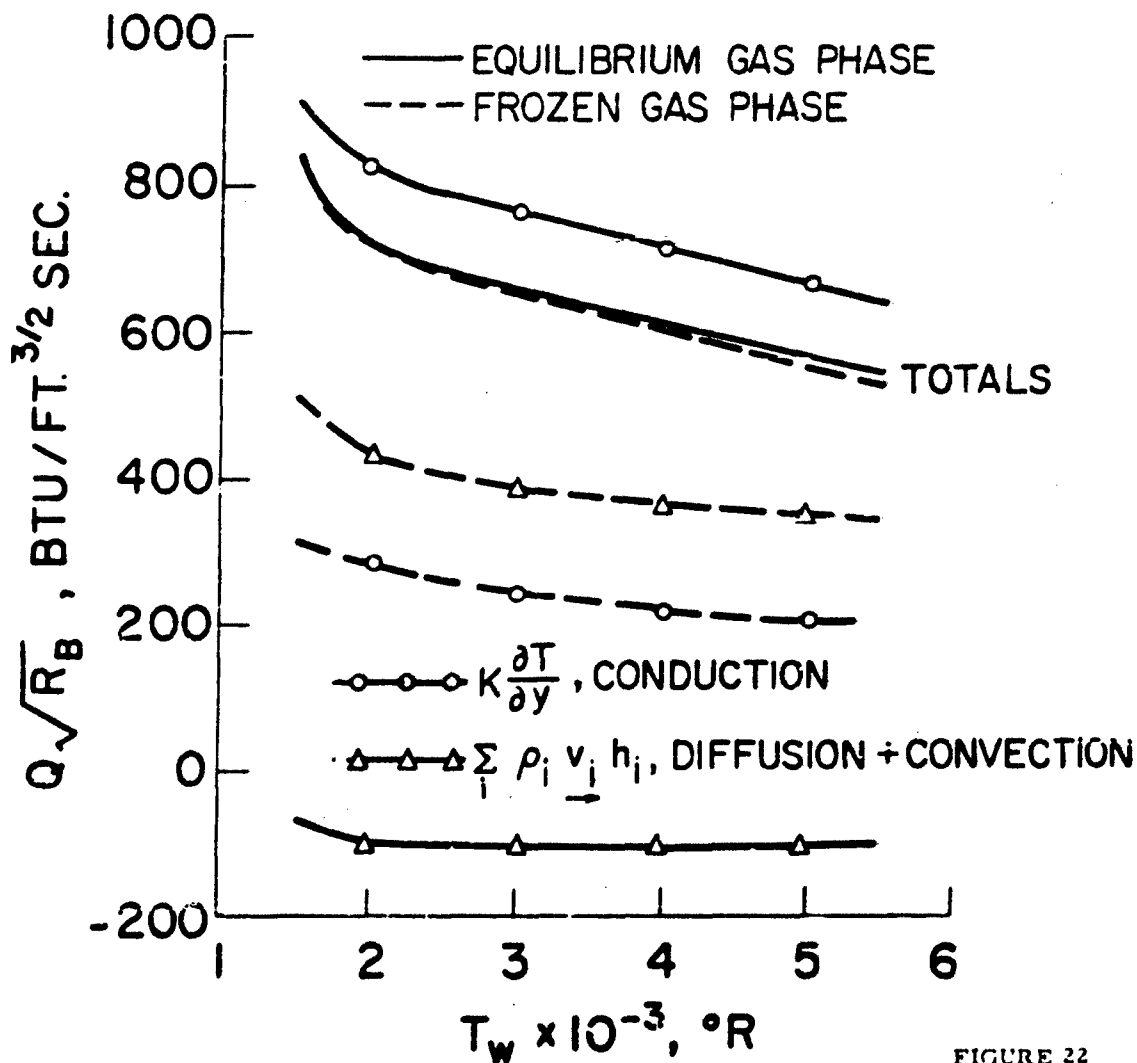
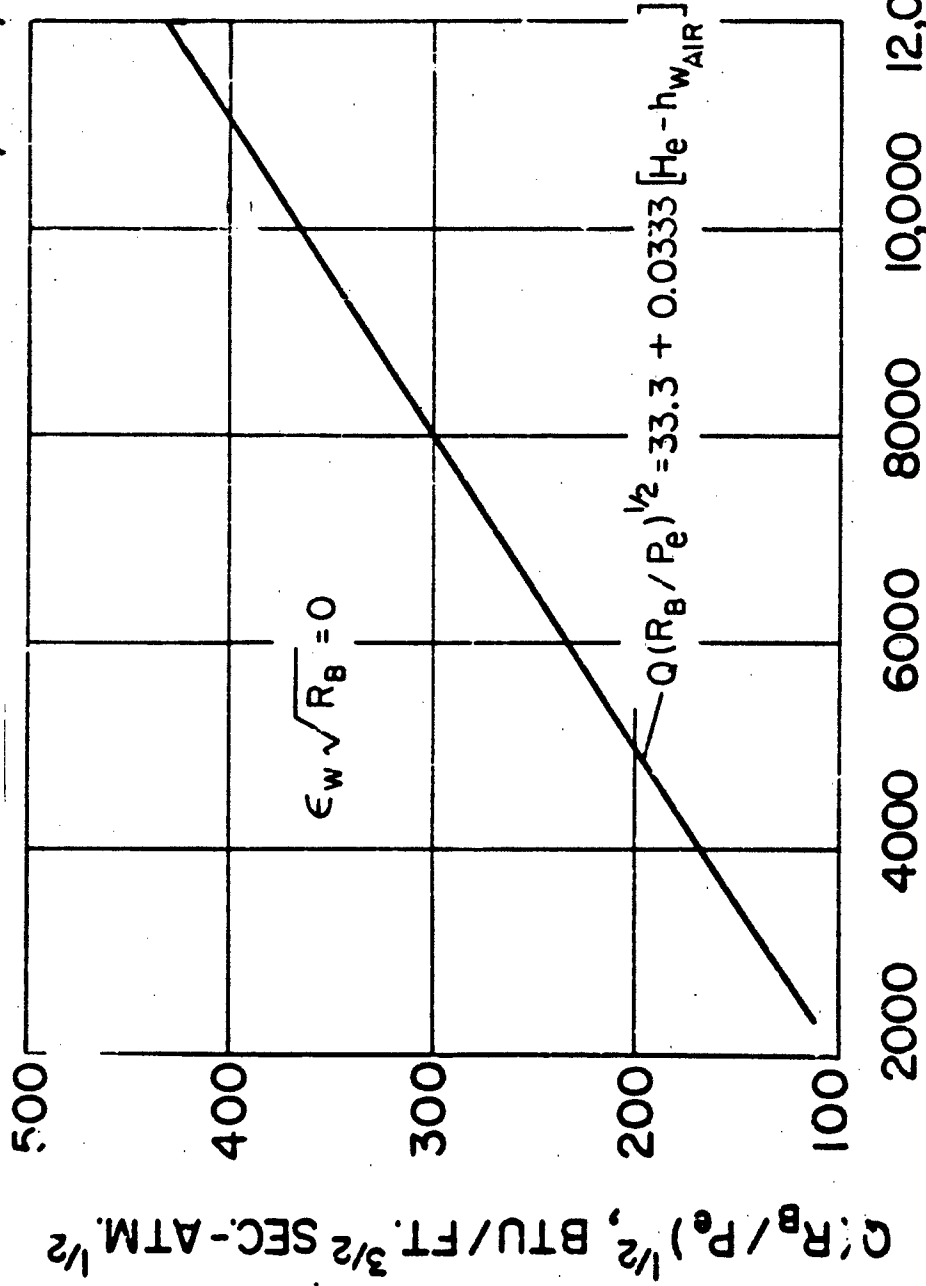


FIGURE 22

HEAT TRANSFER CORRELATION FOR HEAT  
 CONDUCTED INTO SOLID GRAPHITE,  $\Lambda=0, \delta=1$



$[H_e - h_{wAIR}]$ , BTU/LB.

FIGURE 25

# CORRELATED HEAT TRANSFER INTO SOLID GRAPHITE VERSUS SURFACE TEMPERATURE

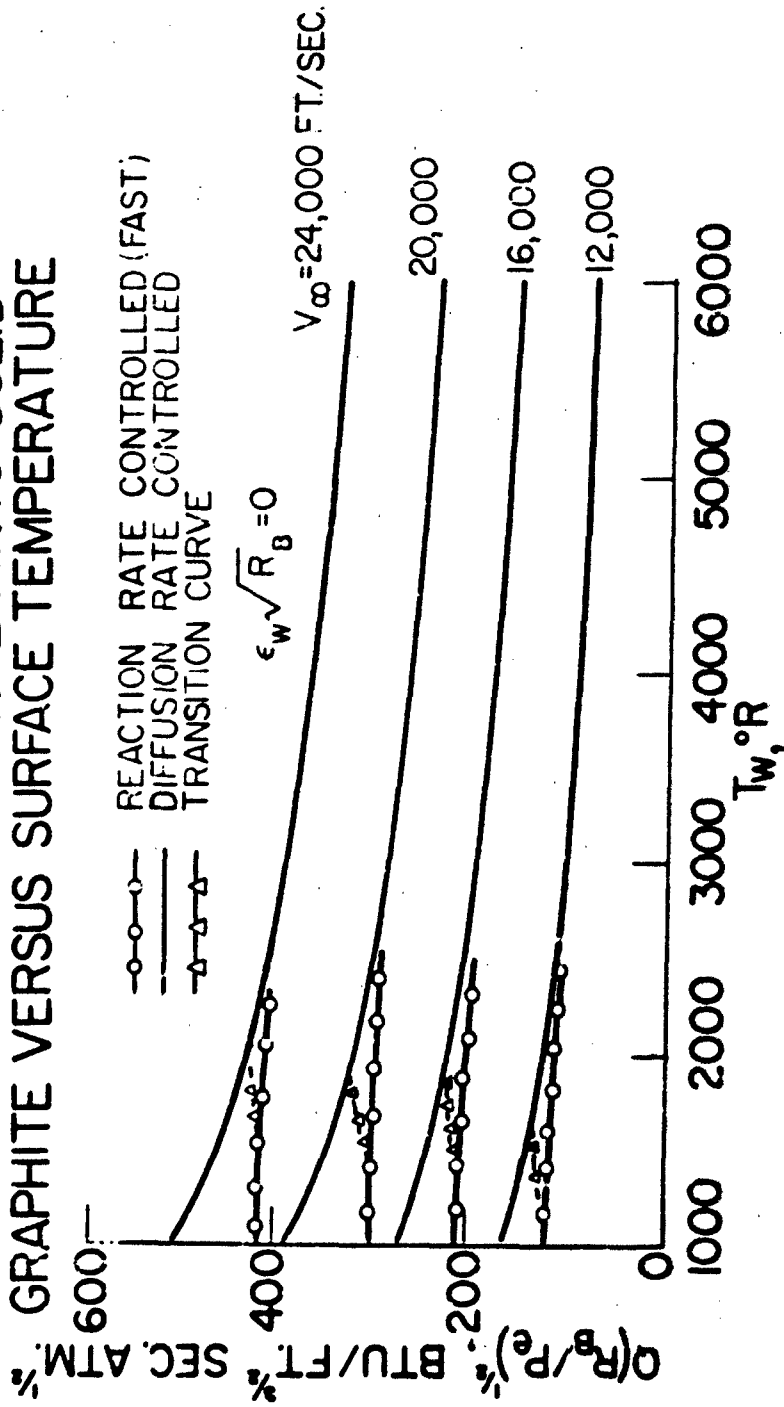


FIGURE 24

THE EFFECTIVE HEAT OF ABLATION FOR GRAPHITE  
 IN THE DIFFUSION RATE CONTROLLED OXIDATION REGIME

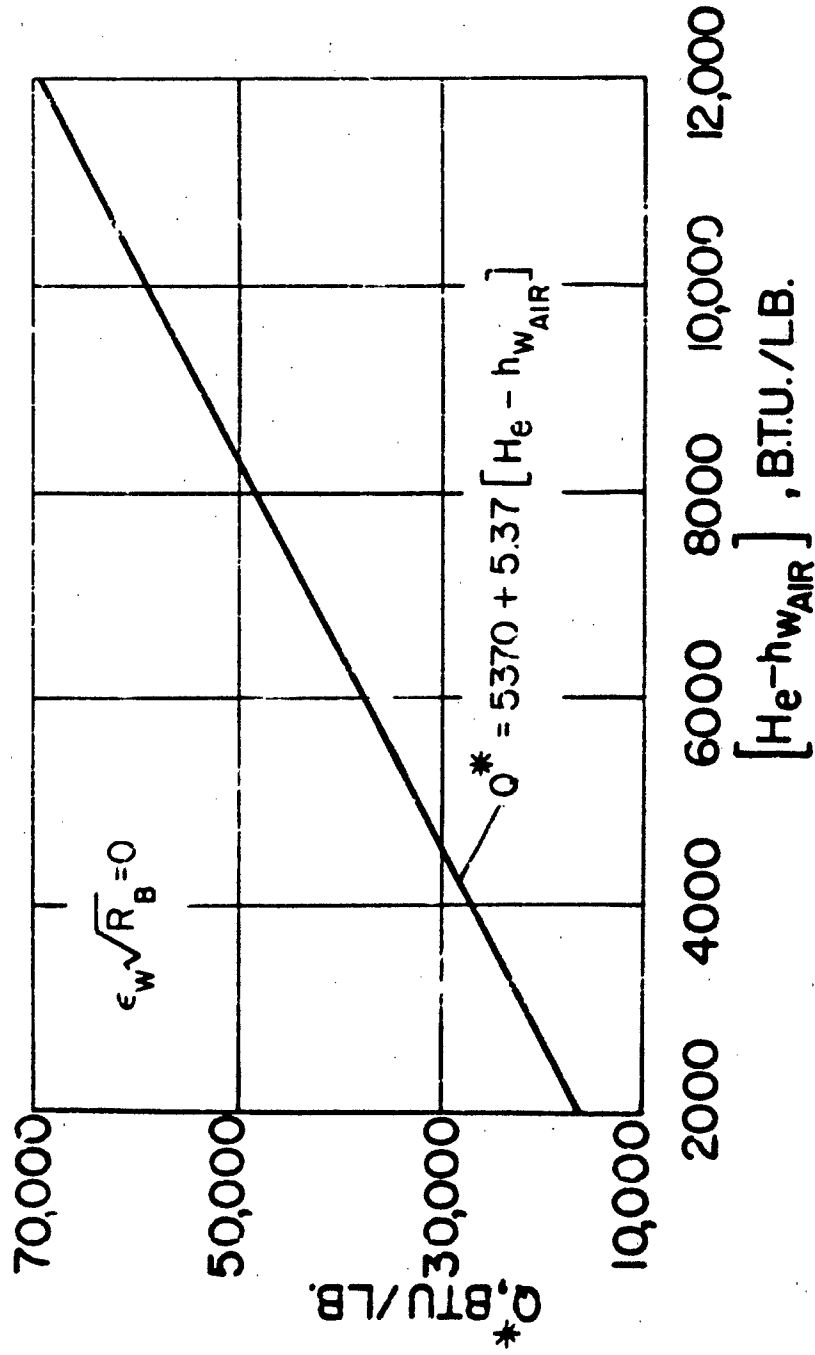


FIGURE 25

# SHEAR FUNCTION FOR A TYPICAL FLIGHT CONDITION

$\Lambda = 0, \delta = 1$

ALT. = 100,000 FT.       $V_{\infty} = 20,000$  FT./SEC.

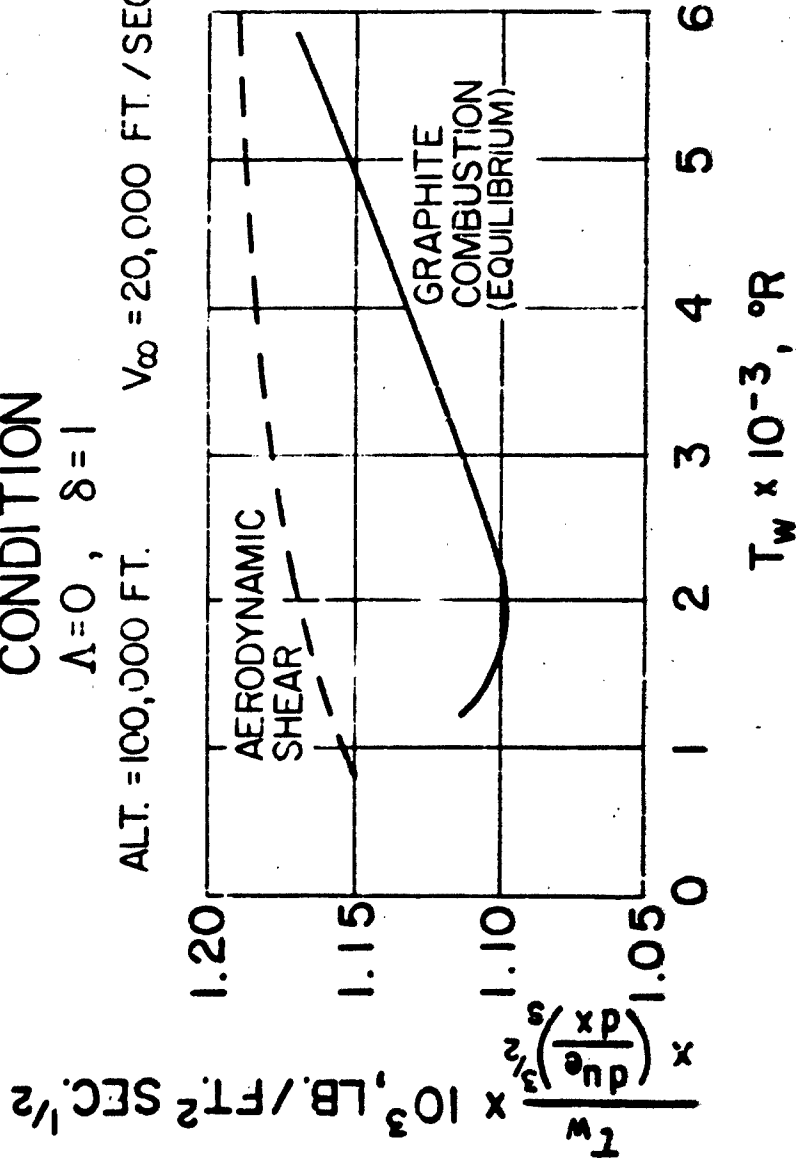


FIGURE 26

# CORRELATED SKIN FRICTION COEFFICIENT

$\Lambda=0, \delta=1$

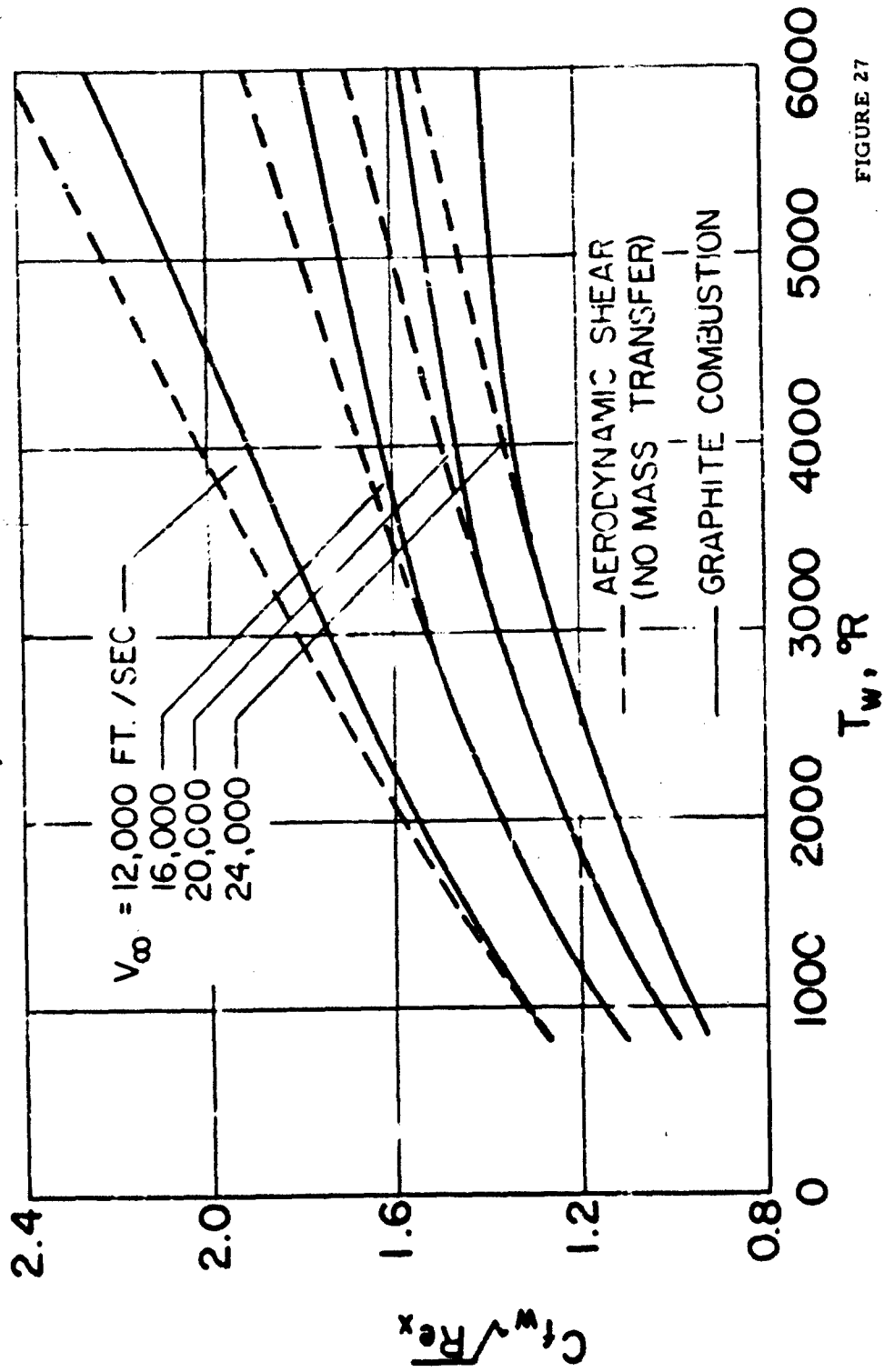


FIGURE 27

# AXIALLY-SYMMETRIC STAGNATION POINT RADIATION EQUILIBRIUM SURFACE TEMPERATURE

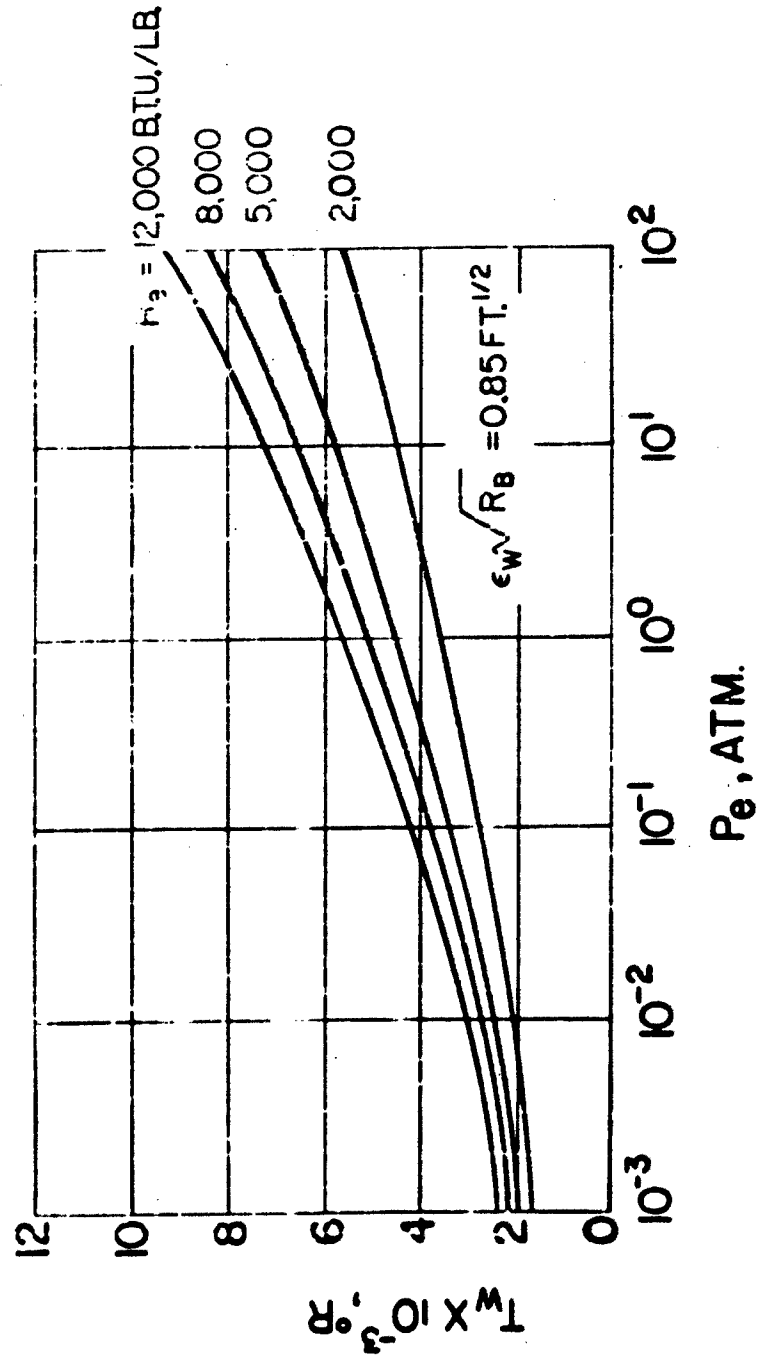


FIGURE 28

SPACE SCIENCES LABORATORY  
MISSILE AND SPACE DIVISION

TECHNICAL INFORMATION SERIES

AUTHOR S. M. Scala	SUBJECT CLASSIFICATION Ablation, Hypersonic Heat Transfer, Graphite	NO. R62SD72
TITLE The Ablation of Graphite in Dissociated Air - Part I: Theory		DATE Sept., 1962
REPRODUCIBLE COPY FILED AT MSO LIBRARY. DOCUMENTS LIBRARY UNIT - VALLEY FORGE SPACE TECHNOLOGY CENTER - RING OF PENNSA, PA		G. E. CLASS I
		GOV CLASS NONE
		NO. PAGES 98
<p><b>SUMMARY</b></p> <p>The effects of the erosion of the construction of graphite in a high speed flow field are investigated. In the transition regime, the transition in the erosion rate is investigated. In the ablation regime, the ablation rate is investigated. The effects of the surface temperature, surface and depends on the surface temperature and the effect of the surface temperature on the erosion rate is investigated.</p> <p>The erosion rate is given by the following equation:</p> $\frac{dW}{dt} = \frac{1}{A} \left[ \frac{G}{\rho} \right] \left[ \frac{D}{\rho} \right] \left[ \frac{D}{\rho} \right]$ <p>The erosion rate is given by the following equation:</p> $\frac{dW}{dt} = \left[ \frac{D}{\rho} \right] \left[ \frac{D}{\rho} \right]$		

By cutting out this rectangle and folding on the center line, the above information can be fitted into a standard card file.

AUTHOR Stanley M. Scala Manager, High Altitude Aerodynamics

COUNTY NUMBER Joseph Fisher Manager, Aerophysics Section